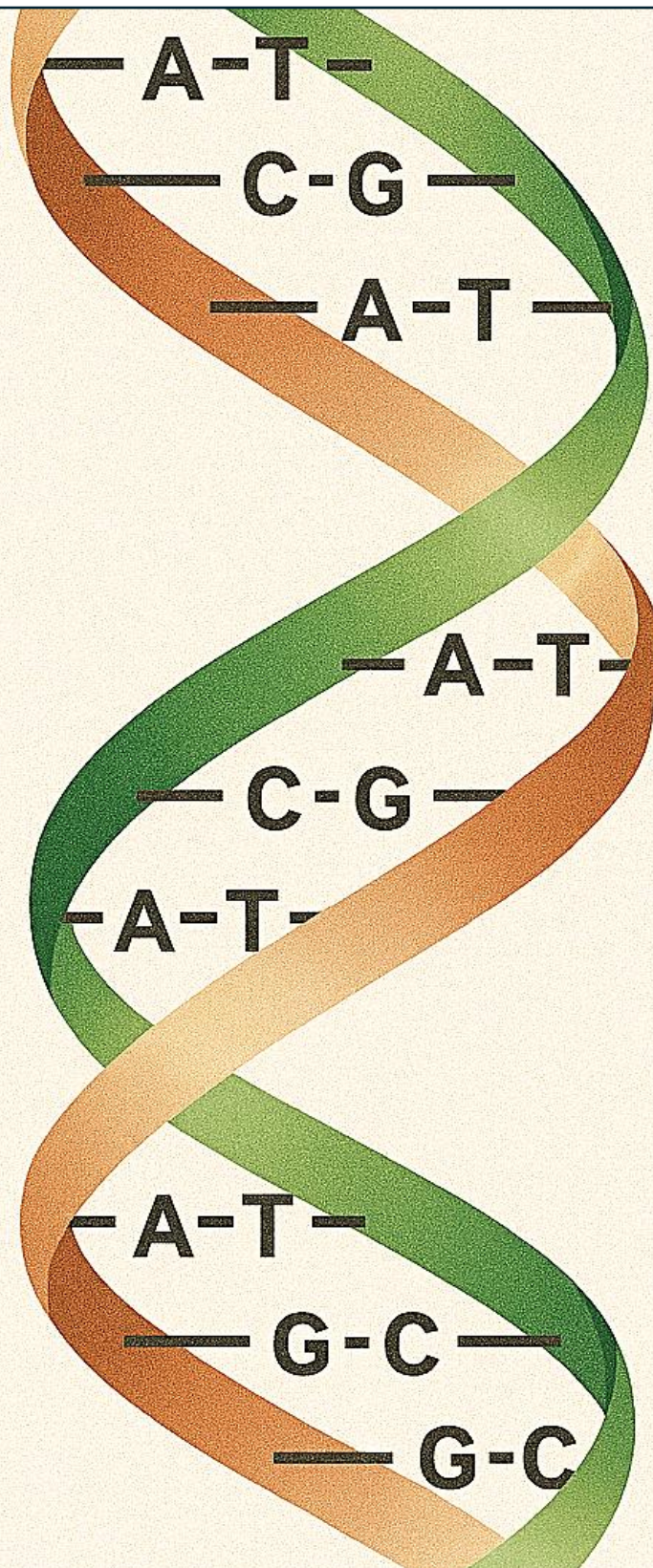




Primed for Editing: Engineering pegRNAs and VLPs to Target LCHADD-Associated Retinopathy

MSc Thesis by Bram Sturkenboom



Primed for Editing: Engineering pegRNAs and VLPs to Target LCHADD-Associated Retinopathy

MSc Thesis by Bram Sturkenboom

Student Number: 1002560

Daily Supervisor: Paul Schürmann

Study Supervisor: Bas Zwaan

Laboratory of Genetics and Fuchs' Group

Wageningen University and Research & Regenerative Medicine Centre Utrecht

03 Sept 2024 – 23 May 2025

Table of Contents

Summary	5
1. Introduction.....	6
1.1. Genetic and Clinical background of LCHADD.....	6
1.2. Current Treatments and Limitations	6
1.3. Prime Editing: A Next-Generation Genome Editing Strategy	7
1.4. Challenges in Prime Editing for Therapeutic Application.....	8
1.5. Engineered Virus-Like Particles for Cell-Targeted Prime Editing	10
1.6. Aim and Hypotheses.....	12
1.6.1. Prime editing Optimization of mHADHA c.1528C>G epegRNA.....	12
1.6.2. Induction of mHADHA c.1528C>G Mutation Using Optimized epegRNA and PE on Genomic Level.....	16
1.6.3. Correcting mHADHA c.1528G>C Mutation via VLP Delivery of epegRNA and PE in Mouse LCHADD Fibroblasts	16
2. Materials and Methods.....	17
2.1. Materials	17
2.2. Methods	18
2.2.1. Molecular Cloning and Genotyping of Plasmids	18
2.2.2. Plasmid Transfection.....	18
2.2.3. Isolating and Genotyping Sorted Cells.....	18
2.2.4. Next Generation Sequencing of DNA Samples	18
2.2.5. Cell Cultures Maintenance	19
2.2.6. PE-eVLP Production	19
2.2.7. PE-eVLP Transduction in Cultured Cells and Genomic DNA Collection	20
2.2.8. PE-eVLP Protein Content Quantification by ELISA	20
2.2.9. In-Fusion Cloning of P4–PE6 Construct.....	20
3. Results.....	21
3.1. FluoPEER Screen of epegRNA and PE System.....	21
3.1.1. Repair-epegRNA and PE Optimization Evaluation	21
3.1.2. Create-epegRNA and PE Optimization Screen Evaluation	23
3.1.3. Impact of Edit Directionality on Prime Editing Efficiency.....	26
3.2. Genomic Analysis of epegRNA-PE System Functionality	27
3.2.1. Induction of mHADHA Mutation in N2a Using Create-epegRNA	27
3.2.2. V3b-VLP-Mediated Delivery of epegRNA into LCHADD Fibroblasts.....	28
4. Discussion and Future Research Recommendations.....	29
4.1. Repair-epegRNA Parameters Impact in FP Screens	29
4.1.1. PBS/RTT Length Impact on Repair-epegRNA Performance	29
4.1.2. Scaffold Impact on Repair-epegRNA Performance	29

4.1.3.	PE variant Impact on Repair-epgRNA Performance	30
4.1.4.	Future Research Regarding Repair-epgRNA Findings.....	30
4.2.	Create-epgRNA Parameters Impact on FP screens	31
4.2.1.	MMR-SM Impact on Create-epgRNA Performance	31
4.2.2.	PE7 Variants Impact on Create-epgRNA Performance	31
4.2.3.	PAM-SM Impact on Create-epgRNA Performance.....	31
4.2.4.	ngRNA Impact on Create-epgRNA Performance.....	32
4.2.5.	Future Research Regarding Create-epgRNA Optimisation	33
4.3.	epgRNA Directionality FluoPEER Screen	33
4.3.1.	Future Research Regarding Findings of epgRNA Directionality	34
4.4.	Inflated MFI in Subset of FluoPEER Screenings	34
4.5.	Mutation Induction in N2a using Create-epgRNA	35
4.5.1.	Future Research Regarding Induction of Mutation in N2a	35
4.6.	Initial Attempts at VLP-Based Prime Editing Delivery.....	35
4.6.1.	eVLP Usage Repair-epgRNA and PE Delivery into LCHADD Fibroblasts	35
4.6.2.	Future Research Regarding eVLP Usage for epgRNA and PE Delivery	36
5.	Acknowledgments.....	37
6.	References.....	38
7.	Appendix.....	43
	Appendix 1	43
	Appendix 2.....	45

Summary

Long-chain 3-hydroxyacyl-CoA dehydrogenase deficiency (LCHADD) is a rare autosomal recessive disorder caused by a c.1528G>C mutation in the HADHA gene, which leads to various symptoms, notably retinal degeneration that manifests in infancy. Current treatments manage symptoms but do not correct the genetic mutation and ultimately fail to prevent vision loss. The aim of this study was to investigate whether prime editing could correct the mHADHA c.1528G>C mutation using engineered virus-like particles as a delivery system in an LCHADD mouse model. The project followed a three-step approach: first, a dual-fluorescent reporter assay (fluoPEER) in HEK293T and N2a cells was used to screen epegRNAs, prime editor (PE) variants, and the effect of mutation repair *versus* induction directionality. Second, genome editing was explored by introducing the mutation into wild-type N2a cells to evaluate epegRNA performance in a genomic context. Third, virus-like particles (VLP) were applied to LCHADD fibroblasts to attempt mutation correction *ex vivo*. The most effective epegRNA design combined the COM scaffold with PE6d, improving editing in HEK293T cells by 93% based on RFP⁺/GFP⁺ count and 204% based on RFP⁺/GFP⁺ MFI. In N2a cells, the same design increased count by 289% and MFI by 98% compared to the epegRNA using the STANDARD scaffold and PEmax. Further experiments explored optimization parameters such as PAM silent mutations, mismatch repair (MMR) silent mutations and ngRNA configurations. While the fluoPEER reporter assay reliably distinguished epegRNA and prime editor performance, editing outcomes at the genomic level were limited. However, using the newly constructed P4-PE6d, VLP delivery of the RNP to mouse LCHADD fibroblasts was inconclusive. Despite these later setbacks, this study demonstrates that epegRNA designs can be systematically optimized and supports the potential of prime editing as a therapeutic strategy for LCHADD.

1. Introduction

1.1. Genetic and Clinical background of LCHADD

Vision loss in childhood profoundly impacts development, independence, and long-term quality of life. Among the many potential causes are inherited metabolic disorders. One such disorder is long-chain 3-hydroxyacyl-CoA dehydrogenase deficiency (LCHADD), a rare autosomal recessive condition that disrupts mitochondrial fatty acid β -oxidation. Most commonly caused by a missense mutation in the HADHA gene (c.1528G>C), this mutation results in a glutamate-to-glutamine substitution (E510Q) in the α -subunit of the mitochondrial trifunctional protein (Neto et al., 2024). This disrupts the final steps of long-chain fatty acid catabolism, leading to toxic metabolite accumulation and energy deficiency during periods of metabolic stress such as fasting or illness, ultimately impairing cellular energy production and contributing to progressive tissue damage, including in the retina (DeVine et al., 2024).

Clinically, LCHADD presents in infancy with hypoketotic hypoglycemia, hepatomegaly, cardiomyopathy, and episodes of metabolic crises. Although dietary interventions, including fat restriction and medium-chain triglyceride supplementation, improve early outcomes, they do not prevent long-term complications such as pigmentary retinopathy (Vockley et al., 2023). This pigmentary retinopathy results in the gradual deterioration of the retinal pigment epithelium (RPE) and its underlying vasculature, eventually leading to irreversible vision loss (DeVine et al., 2024).

Because the genetic cause of LCHADD is so well-defined and most patients carry the same mutation, no effective treatments are yet available for symptoms like the pigmentary retinopathy, a strong case can be made for developing therapies that directly target the underlying mutation.

1.2. Current Treatments and Limitations

Current treatment for LCHADD focuses on managing symptoms and preventing metabolic crises, without correcting the underlying genetic defect. During acute metabolic episodes triggered by fasting, illness, or stress, patients typically receive intravenous fluids containing at least 10% dextrose. This provides immediate energy, suppresses fatty acid oxidation, and prevents the accumulation of toxic metabolites (Prasun et al., 2022; Spiekerkoetter et al., 2009). Long-term management involves dietary measures, specifically a low-fat, high-carbohydrate diet. Long-chain triglycerides are restricted to approximately 5–10% of daily calories, while medium-chain triglycerides provide around 20 to 25% of energy. Essential fatty acids and fat-soluble vitamins are also supplemented to prevent nutritional deficiencies (Rücklová et al., 2021). Although this dietary regimen reduces serious complications such as cardiomyopathy and hypoglycemia, it does not prevent progressive issues such as peripheral neuropathy and retinal degeneration. A recent systematic review of seven clinical studies found that diet and metabolic support often only delay, rather than prevent, retinal damage in LCHADD patients (Maines et al., 2025). More recently, triheptanoin, an odd-chain triglyceride that supplies both acetyl-CoA and propionyl-CoA to support mitochondrial metabolism, has been tested in patients with long-chain fatty acid oxidation disorders (Vockley et al., 2023). While not specific to LCHADD, its reported ability to reduce hospitalization frequency, metabolic crises, and cardiac complications in this broader group suggests that it may offer benefits for LCHADD as well. However, evidence on its efficacy for preventing retinal deterioration is still limited. As a recent case report described a child with severe LCHADD in whom triheptanoin successfully reduced rhabdomyolysis episodes, yet retinal degeneration continued to progress despite treatment (Kahraman et al., 2023). Another recent longitudinal study again showed that visual function continued to decline in LCHADD patients over time, despite adherence to dietary therapy and early clinical intervention (Gillingham et al., 2024). These studies show that despite improvements in survival and crisis management, preventing

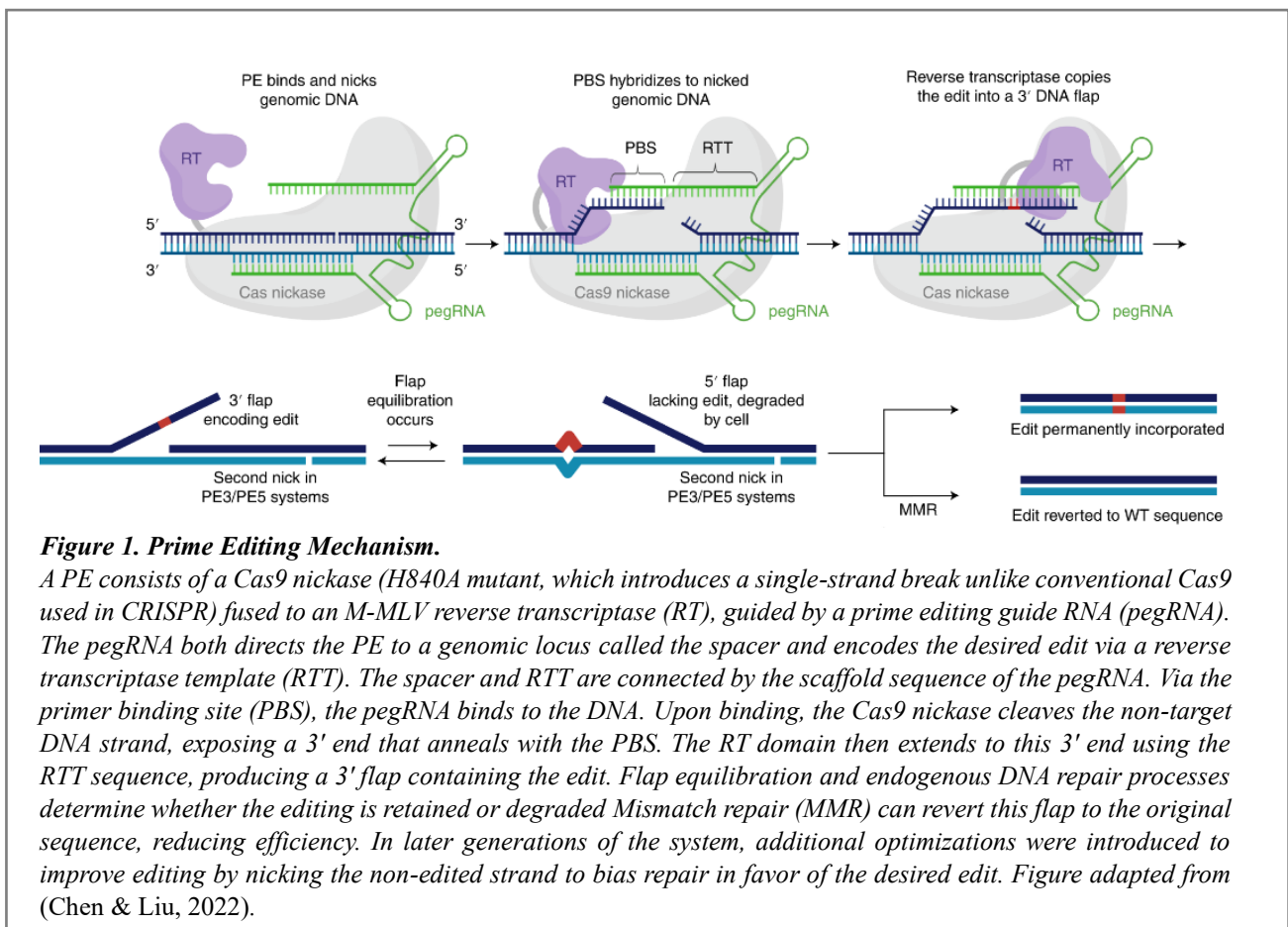
retinopathy remains a significant challenge. This opens the door to next-generation approaches such as prime editing, which offers the potential to directly correct the root cause of LCHADD in RPE cells.

1.3. Prime Editing: A Next-Generation Genome Editing Strategy

Advances in genome editing raise the possibility of interventions for monogenic metabolic diseases such as LCHADD by directly correcting the causative mutation. Traditional CRISPR–Cas9 nuclease editing relies on creating a targeted double-strand break (DSB) and harnessing endogenous DNA repair pathways to introduce sequence changes. However, the DNA break and reliance on homology-directed repair are a risk and pose efficiency challenges, including off-target mutations, chance of imprecise insertions/deletions and unwanted p53-mediated DNA damage response (Haapaniemi et al., 2018; Scholefield & Harrison, 2021).

Given its success in mitigating the effects of several genetic disorders at the post-translational level, mRNA delivery presents itself as a plausible candidate for LCHADD and an alternative to CRISPR–Cas9. But as mRNA delivery is non-corrective in nature, it will require repeated subretinal injections, with attendant risks like retinal detachment (Sharma & Paschalis, 2022), and particularly impractical and distressing for infant patients.

Prime editing offers a more precise alternative, it edits DNA without making a DSB, avoiding many of the risks that come with traditional CRISPR methods (Doman et al., 2022) (Figure 1).



The prime editing mechanism allows for precise insertion of point mutations, small insertions, or deletions, while keeping unwanted by-products to a minimum (Doman et al., 2022). Base editing, a related approach, has been successful for fixing certain single-nucleotide variants, but it comes with a key limitation: it can only perform transition mutations, such as changing A to G or C to T. It cannot make transversions, such as the C to G substitution that causes LCHADD. Since no base editor currently exists that can perform this type of change, and prime editing has shown strong potential for high editing efficiency, it stands out as a promising strategy to directly correct the c.1528G>C HADHA mutation in LCHADD RPE cells.

1.4. Challenges in Prime Editing for Therapeutic Application

Prime editing offers a promising way to correct the c.1528G>C mutation in LCHADD, but how well it works really depends on the pegRNA design. Earlier studies have shown that prime editing performance can vary a lot between different cell types, and that when the engineered pegRNA (epegRNA) is not well-designed, the 3' extension can become unstable or get degraded before it even has a chance to work (Nelson et al., 2022). To figure out which epegRNA designs work best, the designs must be tested empirically on cell cultures. Traditionally done by genomic sequencing, this method can be time consuming. A quick method to screen epegRNAs is the Fluorescent Prime Editing and Enrichment Reporter assay (Figure 2). This is a fluorescent reporter assay that incorporates a specific target sequence and uses fluorescence to indicate editing activity. It has been shown that fluoPEER (FP) screening can help identify the most effective pegRNA designs for correcting disease mutations, even in patient-derived cells. Upon successful co-transfection of the epegRNA, PE and FP plasmid, the system not only reports transfection efficiency but also provides a direct readout of editing activity. Because it enriches for truly edited cells, FP can yield up to a threefold increase in editing signal compared to conventional transfection-based selection alone (Schene et al., 2022). This makes FP a good method screening various epegRNA optimisations and prime editors.

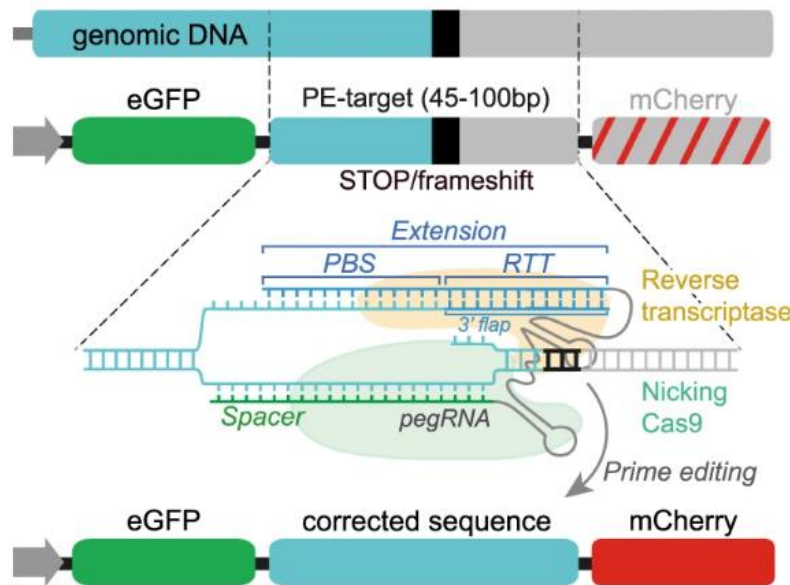


Figure 2. Schematic overview of the FP dual-fluorescent reporter system.

The plasmid construct contains CMV-driven expression units for eGFP, a PE target sequence, and mCherry. Under default conditions, only eGFP is expressed due to the presence of a stop codon within the inserted 45–100 bp mHADHA-derived target sequence (replacing the original mHADHA c.510 CAA codon). Upon successful prime editing, the pegRNA and PE correct the inserted sequence, restoring the open reading frame and enabling mCherry expression. This provides a direct fluorescence-based readout of editing efficiency. This readout can be read as relative RFP⁺/GFP⁺ count, based number of RFP⁺ and GFP⁺ cells, and relative RFP⁺/GFP⁺ MFI (relative mCherry/GFP). The exact inserted target sequences used in this study are provided in Supplementary information 1. Figure adapted from (Schene et al., 2022).

A second challenge lies in the delivery of the prime editing components to the RPE cells. The full prime editing system includes a Cas9 nickase fused to a reverse transcriptase (about 6.3 kb), plus one or more guide RNAs. This protein complex, the ribonucleoprotein (RNP), is too large for common viral vectors such as adeno-associated virus (AAV), which can only carry about 4.7 kb. Earlier research tried to work around this problem using dual-AAV systems or smaller, trimmed-down versions of Cas9, but these approaches often come at the cost of efficiency (Jang et al., 2021). Moreover, AAV-mediated delivery of the prime editing system will result in long-term, non-transient expression of the editing enzymes, which poses significant safety concerns. As the sustained expression of the Cas9-RT fusion protein and epegRNA can increase the risk of off-target edits, genomic instability, or immune responses, this makes AAV-mediated delivery undesirable for targeting the c.1528G>C HADHA mutation in LCHADD RPE cells. Interestingly, AAV vectors have already been used to treat LCHADD in a relevant LCHADD mouse model. This has been done via delivery of a functional HADHA gene, which avoids the risk of delivering a prime editing system and thus avoids prolonged editor expression (Babcock et al., 2024). However, even this method is not without risks. AAV-delivered DNA can sometimes integrate randomly into the host genome, raising concerns about insertional mutagenesis and long-term safety (Deyle & Russell, 2009).

One possibility is to deliver the RNP via lipid nanoparticles (LNPs). They've shown promise in other areas of genetic medicine, and in theory, could help get the RNP into the RPE cells without relying on viral vectors. A common downside of LNP delivery is its liver tropism, as systemically administered LNPs tend to accumulate mostly in the liver (with an estimated 30–90% of the dose ending up in hepatic tissue) (Lu et al., 2024). However, this liver tropism can be mitigated via local injections, and has been done before with the delivery of mRNA to the RPE (Patel et al., 2019). However, even with local administration, LNP-mediated transfection of RNP is difficult. LNP formulations are optimized for

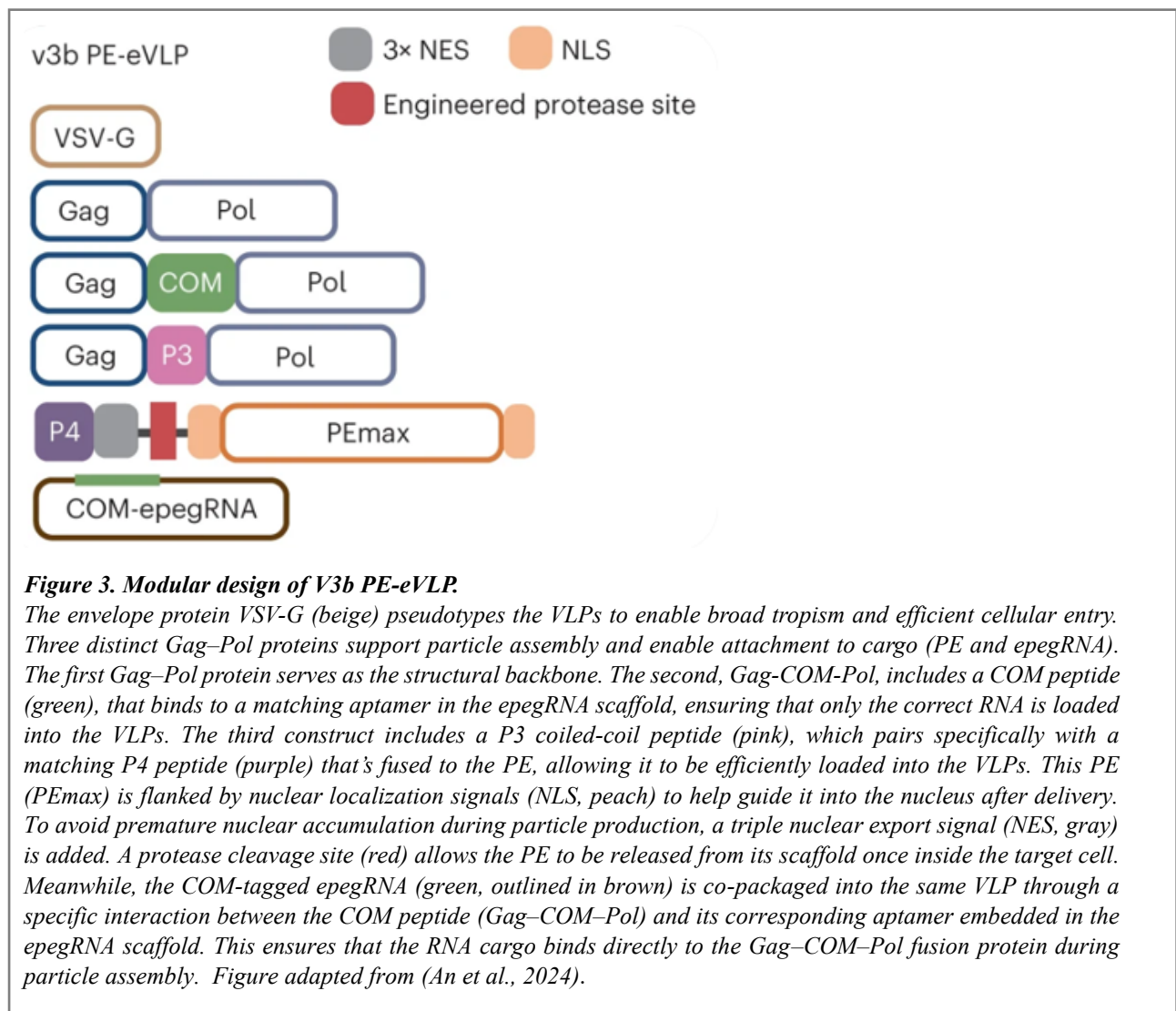
mRNA and face significant challenges in encapsulating and delivering large molecules due to size limitations (Chai et al., 2025). Furthermore, endosomal escape poses a major obstacle for LNP-based RNP delivery. Unlike mRNA, which is functional in the cytoplasm, the large RNP complex used in prime editing requires both endosomal escape and subsequent nuclear import. LNPs have poor efficiency in this regard, with the vast majority of internalized RNPs being degraded before reaching their genomic targets (Chatterjee et al., 2024). Even when escape is successful, the intact nuclear envelope in non-dividing cells like RPE presents an additional barrier. Without cell division to transiently disrupt the nuclear membrane, nuclear access relies on active transport mechanisms, which are often insufficient for large synthetic complexes like RNPs (Dean et al., 2005). These reasons leave LNP an undesirable candidate for delivery of the epegRNA and PE.

With most traditional delivery strategies falling short, either due to safety concerns, tissue specificity, or inefficiency, VLPs have become one of the few practical alternatives left for delivering PEs to RPE cells. VLPs offer a way to package the PE and epegRNA plasmids in a form that is both transient and targeted, without the long-term expression risks associated with viral vectors.

1.5. Engineered Virus-Like Particles for Cell-Targeted Prime Editing

VLPs are self-assembling, enveloped protein shells typically derived from retroviral or lentiviral capsid proteins, but engineered to exclude any viral genome, thereby producing non-replicating and integration-free vectors (Mohsen & Bachmann, 2022). These particles are generated by transfecting producer cells (HEK293T gesickles) with plasmids encoding the viral structural proteins and the desired cargo, such as PE proteins and guide RNAs. Once produced, the particles bud from the cell, self-assemble and envelop the DNA and deliver the cargo to target cells without persistent expression or integration-related risks (An et al., 2024).

Earlier versions of RNP delivery using VLPs have been done using base editors, targeting the *RPE65* mutation in RPE cells. This early approach achieved 21% correction of the *RPE65* mutation and restored expression of the target protein (Banskota et al., 2022). More recently, prime editor VLPs (PE-eVLPs) were developed, with the third-generation variant (v3b PE-eVLPs) (Figure 3), achieving clinically relevant editing in a mouse model of inherited retinal disease. A single subretinal injection of v3b PE-eVLPs carrying the prime editing RNP resulted in an average editing rate of 7.2% in *RPE65* in RPE cells, sufficient to partially restore visual function (An et al., 2024).

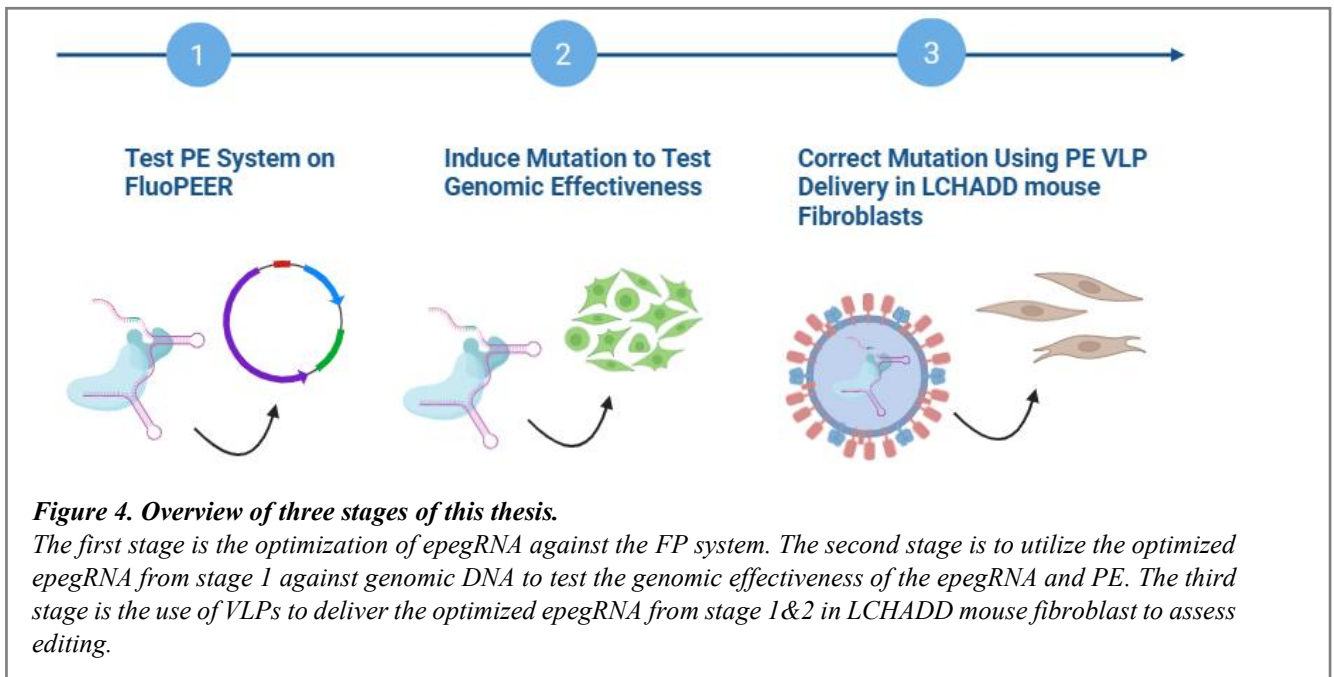


One of the issues facing VLP usage, is that because VLPs are built from viral proteins, they can still trigger immune responses, even though they carry no viral genome, which could be especially damaging in the context of already stressed RPE cells (Chew et al., 2016; Shirley et al., 2020). To mitigate this, An et al. describes the possibility of a single-dose of RNP PE-eVLPs delivery, which may mitigate clinically relevant immunogenicity. This claim however needs further investigation, as stated by the authors (An et al., 2024).

Despite the possible risk of immune responses, the ability of VLPs to deliver gene editors transiently and without integration, combined with early successes in the eye, makes this approach a compelling path forward for treating inherited retinal disorders like LCHADD.

1.6. Aim and Hypotheses

Given the above considerations, this study develops and evaluates key components of a prime editing–based therapeutic strategy for LCHADD, focusing on optimization of epegRNAs and delivery using VLPs. While the ultimate aim is to evaluate this genome editing strategy in a disease-relevant mouse model *in vivo*, the current project focuses on *in vitro* optimization in HEK293T and N2a, but also using LCHADD fibroblasts derived from a HADHA-deficient mouse model. The experimental approach was structured in several stages (Figure 4).



1.6.1. Prime editing Optimization of mHADHA c.1528C>G epegRNA

The first stage of this study focused on optimizing the prime editing system for correcting the mHADHA c.1528G>C mutation. Multiple epegRNAs and PE variants were tested using the FP reporter assay in HEK293T and N2a cells, which are commonly used in prime editing experiments due to their high transfection efficiency and robust editing response. Although RPE cells would have been more biologically relevant to the disease context, they were excluded from this initial FP screening stage due to consistently undetectable FP signal, indicating extremely low editing activity. A range of editing parameters were tested, as summarized in Table 1. This included not only conventional repair-epegRNAs designed to revert the c.1528G>C mutation, but also so-called create-epegRNAs that introduce the same mutation into wild-type cells. The rationale for testing both directions of editing is discussed in a later section.

Table 1. Overview of screening parameters designed to optimize the epegRNA targeting mHADHA Exon 15. Each parameter is listed with its design rationale and the specific configurations tested. The genomic positions of PAM-disrupting silent mutations (PAM-SM), MMR-evading silent mutations (MMR-SM), and ngRNA target sites are shown in Figure 5, which provides a spatial reference for all engineered variants. Screens included variation of PBS/RTT lengths, epegRNA scaffold structures, PE variants, PAM-disrupting silent mutations, mismatch repair–evading silent mutations, and nicking guide RNAs targeting the non-edited strand. Complete sequence designs are provided in Supplementary information 1. Transfection details provided in the Material & Methods.

Screen Type	Design Purpose	Design Category	Variant tested
PBS and RTT length	Optimize reverse transcription priming (Anzalone et al., 2019)	Mutation Correction (“Repair”)	PBS length of 8 till 12 in combination with RTT length of 34 and 35
PE variant	Evaluate editing efficiency per PE type (Anzalone et al., 2019)	Mutation Correction (“Repair”)	PEmax, PE6a till PE6g, PEtrunc
	(Yan et al., 2024)	Mutation Induction (“Create”)	PE7, PE7-Vpe and PE7-P2A-MLH1 dn
epegRNA scaffold	Assess the impact of scaffold modifications on editing efficiency	Mutation Correction (“Repair”)	COM-Standard-MS2-F+E scaffold
ngRNA	Test enhanced strand nicking and editing rate (Nelson et al., 2022)	Mutation Correction (“Repair”) / Mutation Induction (“Create”)	ngRNA1–ngRNA7
MMR-evading silent mutations	Improve edit retention via MMR evasion (Chen & Liu, 2022)	Mutation Induction (“Create”)	- CTA>CTG - CTA>TTG - CTA>CTC - CTA>TTA - CTA>CTT
PAM-disrupting silent mutations	Prevent post-edit re-cutting (Anzalone et al., 2019)	Mutation Induction (“Create”)	- TGG >TCG - TGG >TTG - TGG >TAG
Repair vs. Create comparison	Distinguish edit directionality	Comparative	

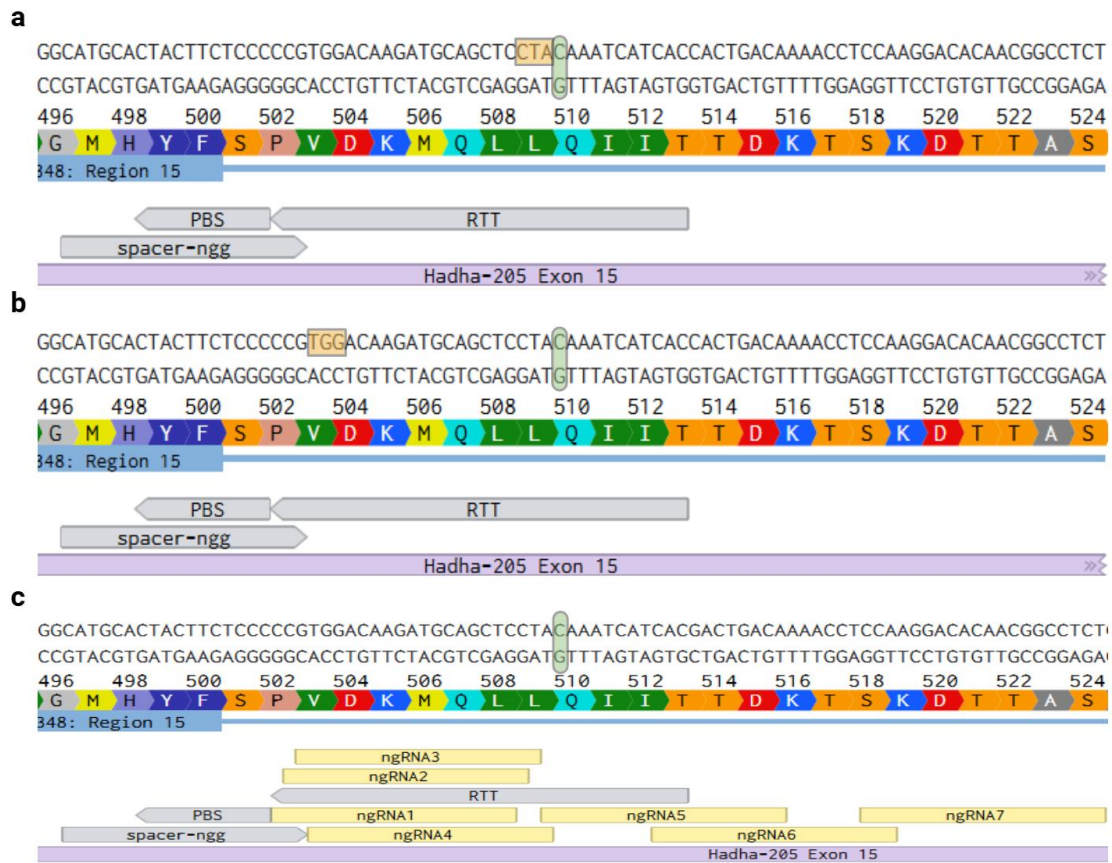


Figure 5. Genomic Localization of MMR-SM, PAM and ngRNA target sites for Prime Editing at mHADHA Exon 15. Amino acids are colour-coded, and the location of the target nucleotides is boxed in green. **a** Sequence map showing the position of MMR-SM introduced at codon 510 (highlighted CTA codon in yellow). These variants (e.g., CTA>CTG, CTC, etc. see Table 1) were designed to improve edit retention by reducing MMR activity at the target site. **b** Localization of the protospacer adjacent motif (PAM) downstream of the editing site (in yellow). PAM-SM (e.g., TGG>TCG, TAG, TTG see Table 1) were introduced to prevent Cas9 re-cutting following successful editing. **c** Mapping of nicking guide RNA (ngRNA) (ngRNA1–ngRNA7, see Table 1) target sites relative to the epegRNA RTT and PBS.

The justification for the selected PBS and RTT lengths was guided by both prior epegRNA design literature and the spatial constraints imposed by the c.1528G>C target site. While earlier protocols recommended a PBS length of around 13 nucleotides (Anzalone et al., 2019), more recent high-throughput data suggest that 11–12 nucleotides may be more effective, depending on RTT length (Yu, Kim, Park, Kwak, et al., 2023). Because of only one NGG pam sight allowing for proper spacer positioning (Figure 5b) and given that flap resolution requires at least 7–10 nucleotides of RTT homology beyond the edit, shorter RTTs would not sufficiently span the required distance (Anzalone et al., 2019; Nelson et al., 2022). Based on this information, it was hypothesised that the larger PBS lengths would outperform the shorter PBS lengths.

To assess the impact of epegRNA scaffold architecture on editing efficiency, four scaffold designs were tested that represent successive innovations in prime editing guide RNA engineering. The first scaffold, the STANDARD scaffold, contains no stabilizing modifications and serves as the minimal baseline (Anzalone et al., 2019). The MS2 scaffold incorporates two MS2 aptamer hairpins (An et al., 2024, Cell), enabling RNA–protein interactions with MS2 coat proteins originally designed for VLP packaging (An et al., 2024). The F+E scaffold retains the minimal backbone but adds two key features: a “flip” (F) mutation and an extended stem-loop (E) that improve Cas9–pegRNA complex formation and reduce premature Pol III termination, both designed to increase editing efficiency (Nelson et al., 2022). Finally, COM scaffold retains the F+E backbone, but instead of the bulky MS2 aptamer of the MS2 scaffold, it incorporates a more compact RNA aptamer. Also designed for VLP packaging, this more compact RNA aptamer binds the Gag-Com-Pol protein (Figure 3). This reduction in size should minimize sequence burden and steric hindrance, improving both guide stability and VLP compatibility (An et al., 2024). It is thus hypothesized that the COM scaffold would yield a higher editing efficiency than other scaffolds, as the scaffolds tested are all an “upgrade” of each other, the hypothesized ranking of editing efficiency was COM>F+E>MS2>STANDARD.

To evaluate how PE architecture influences editing efficiency, several Cas9–reverse transcriptase (RT) fusion variants were tested. The baseline editor, PEmax, is an improved version of PE2 with enhanced nuclear localization signals and an optimized nCas9 domain, enabling precise genome editing without inducing double-stranded DNA breaks. The PE6 family (PE6a–PE6g) modifies the RT domain to improve template processivity, reduce premature termination, and enhance flap resolution. PE6a and PE6b incorporate compact RTs derived from bacterial retrons (Ec48) and yeast retrotransposons (Tf1), respectively, reducing the overall size of the construct. PE6c combines mutations from both PE6a (Ec48) and PE6b (Tf1) to the RT, that further stabilize the RT–template interaction, which should improve editing performance on GC-rich or structured RTTs. PE6d retains the M-MLV RT backbone from PEmax but includes improved edits that reduce fall-off and increase the generation of full-length DNA flaps. PE6e, PE6f, and PE6g incorporate further point mutations in both the RT and Cas9 domains, aiming to refine polymerase kinetics and editing efficiency (Doman et al., 2023). Finally, PEtrunc is a size-reduced version of PEmax, developed for packaging into AAV vectors by truncating the RT domain (Gao et al., 2022). More recently, PE7 was introduced by fusing PEmax with the RNA-binding exonuclease protection factor La. This addition stabilizes epegRNAs by binding to their poly-U regions, significantly improving editing efficiency across diverse targets and cell types. PE7-P2A-hMLH1dn was also evaluated, being a co-expression PE7 and a dominant-negative MLH1 variant. This MMR-inhibitor should enhance edit retention (Yan et al., 2024). Finally, PE7-vPE was tested, a new generation PE designed to reduce indels (Chauhan et al., 2024).

Several hypotheses can be made about PE performance. All tested variants are expected to outperform PEmax, given the design improvements across newer generations. Since PE7 and its derivatives are the most recently developed, it is reasonable to hypothesize that they outperform earlier PEs, with PE7-P2A-hMLH1dn likely showing the highest efficiency in N2a cells due to its ability to inhibit mismatch repair. Still, because editing outcomes are highly dependent on the specific cell type and target locus, predicting a full performance ranking is difficult. PE6c is expected to perform better than PE6a and PE6b, as it combines the most effective features of both. For PE6e, PE6f, and PE6g, however, their improvements are more general and not tailored to a specific application, so their effectiveness will have to be determined experimentally.

The selection of PAM-SM RTTs, MMR-SM RTTs, and ngRNAs was based on initial feasibility and strategic positioning around the target site. The choice of PAM-SMs was highly constrained, as only substitutions in the second base of the PAM-overlapping codon can preserve the original amino acid sequence. For MMR-SM RTTs and ngRNAs, we selected a limited number of candidates that appeared promising based on their sequence context and proximity to the edit site, which is advised in previous

studies (Chen & Liu, 2022), it was thus hypothesized that the MMR-SMs and ngrRNAs closest to the edit site would outperform those more distant to the edit site.

1.6.2. Induction of mHADHA c.1528C>G Mutation Using Optimized epegRNA and PE on Genomic Level

The second stage was to assess genome-level editing performance beyond the FP reporter assay. The most effective epegRNA–PE combination was tested in a cellular model. As LCHADD model cells were not yet available, the c.1528G>C mutation was introduced into wild-type N2a cells to simulate the disease context. This mutation-induction strategy was proposed as a functional proxy for evaluating the activity of the c.1528C>G-targeting epegRNA. It was hypothesized that successful detection of the mutation via sequencing would confirm the editing capability of the selected epegRNA-PE combination. Furthermore, once LCHADD model cells became available, only a single nucleotide substitution in the pegRNA would be required to shift from mutation induction (create-epegRNA) to correction (repair-epegRNA), while preserving all prior optimizations. N2a cells were chosen due to their murine origin, aligning with the project’s focus on the mHADHA locus. Transfection conditions are detailed in the Materials & Methods section.

1.6.3. Correcting mHADHA c.1528G>C Mutation via VLP Delivery of epegRNA and PE in Mouse LCHADD Fibroblasts

In the final stage, the optimized PE and epegRNA were delivered to mouse-derived LCHADD fibroblasts harbouring the mHADHA c.1528G>C mutation using previously validated V3b-VLPs. These fibroblasts, isolated from a knock-in mouse model carrying the human HADHA c.1528G>C variant, represent a disease-relevant *ex vivo* system for assessing editing efficacy at the genomic level. This mouse model replicates key aspects of human LCHADD, including early-onset retinal degeneration and progressive metabolic dysfunction (Gaston et al., 2023). Importantly, retinal pathology develops even in the absence of metabolic crises, suggesting a tissue-intrinsic effect of the mutation. Longitudinal analysis further reveals age-dependent worsening of retinal structure and function, closely paralleling disease progression in humans (Babcock et al., 2024). The use of these fibroblasts thus provides a robust platform for evaluating therapeutic delivery strategies such as VLPs in a context that closely mirrors the human disease phenotype.

2. Materials and Methods

2.1. Materials

Plasmids used in this study were obtained from Addgene and included Gag–COM–Pol (Addgene #211373), COM-epgRNA–Dnmt1 (Addgene #211376), and P4–PE (Addgene #211375), originally described in (An et al., 2024). Further plasmids used were pMD2.G (Addgene #12259) (VSV-G), wild-type Moloney Murine Leukemia Virus (MMLV) pBS-CMV-gagpol (Addgene #35614), gag-P3-pol plasmid (Addgene #211374) and engineered Gag–PE fusions were also utilized for virus-like particle (VLP) production. For VLP concentration, PEG-it Virus Precipitation Solution (System Biosciences, LV825A-1) and phosphate-buffered saline (PBS) were used. PVDF syringe filters (0.45 µm; Merck Millipore) were used for sterilization. The dual-fluorescent FP reporter plasmid vector pmGFP-P2A-K0-P2A-RFP (Addgene #105686) was used as a FP backbone. Competent *E. coli* Stellar™ cells (Takara Bio) were used for all cloning and propagation steps. For epgRNA assembly, oligonucleotides were synthesized by Integrated DNA Technologies (IDT, USA). epgRNA constructs were cloned into the pU6-pegRNA-GG-acceptor vector (Addgene #132777), which was linearized by digestion with BsaI-HFv2 (New England Biolabs, R3733S) according to the manufacturers protocol. ngRNA constructs were cloned into the pFYF1320 EGFP Site#1 vector (Addgene #47511). The In-Fusion® HD Cloning Kit (Takara Bio, #638910) was used for directional cloning into the P4-PE vector (Addgene #211375). Vector linearization was performed using SapI (NEB, R0569S) and XhoI (NEB, R0146S) in 10× rCutSmart™ Buffer (NEB, B6004S), followed by final ligation using the In-Fusion HD Enzyme Premix provided in the kit. To generate enough high-purity plasmid DNA from liquid bacterial cultures, the PureLink™ Quick Plasmid Miniprep and Midiprep Kits (Thermo Fisher Scientific) and the NucleoBond Xtra Midi/Maxi Kits (Macherey-Nagel) were used, depending on the required scale. LB agar plates supplemented with either kanamycin or ampicillin (both from Sigma-Aldrich) were used for bacterial selection, depending on the resistance marker of the plasmid.

Cell lines used in this study included Human Embryonic Kidney cells (HEK293T; ATCC CRL-3216), mouse neuroblastoma cells (Neuro-2a; ATCC CCL-131), and Gesicle Producer 293T cells (Takara, 632617). All cell lines were cultured in Dulbecco's Modified Eagle Medium (DMEM; Gibco, 11965092) supplemented with 10% fetal bovine serum (FBS; Gibco, 10270106) and 1% penicillin-streptomycin (Gibco, 15140122). For mouse fibroblast cultures, DMEM/F-12 Nut Mix (Ham) medium (Gibco, 11320033) supplemented with 10% FBS and PenStrep (1×, Gibco) was used. Transfections were performed using Lipofectamine 2000 (Invitrogen, 11668019). Phosphate-buffered saline (PBS; Gibco) was used for cell washing and handling procedures. Genomic DNA was extracted using the Quick-DNA Microprep Kit (Zymo Research, D3020), following the manufacturer's instruction, using lysis buffer composed of Tris-HCl, SDS, and proteinase K (Sigma-Aldrich, P2308). PCR amplification was conducted using Phusion U Green Multiplex PCR Master Mix (Thermo Fisher Scientific, F564S), and amplicons were purified with the QIAquick Gel Extraction Kit (Qiagen, 28704) or equivalent. DNA concentration was measured using a Qubit 4 Fluorometer (Thermo Fisher, Q33226) and the dsDNA HS Assay Kit (Thermo Fisher, Q32851). Genomic DNA samples were submitted to MacroGen Europe (Amsterdam, The Netherlands) for library preparation and sequencing. Next generation sequencing (NGS) sequencing libraries were prepared using genomic DNA with the Extracta™ DNA Prep kit (QuantaBio, 95091-025). Flow cytometry was performed on a CytoFLEX S (Beckman Coulter), with data analysed using CytExpert software and GraphPad Prism (GraphPad Software, USA).

2.2. Methods

2.2.1. Molecular Cloning and Genotyping of Plasmids

All plasmids were assembled using Golden Gate cloning. DNA fragments were PCR-amplified using Q5® High-Fidelity DNA Polymerase (New England Biolabs, M0491S) according to the manufacturer's instructions (Primers found in Supplementary information 1). The resulting plasmids were transformed into *Escherichia coli* Mach1 chemically competent cells (Thermo Fisher Scientific, C862003). Following transformation, cells were cultured overnight in selective LB media containing appropriate antibiotics (1:1000): ampicillin for epegRNA plasmids (carrying a β -lactamase resistance gene) and kanamycin for FP (carrying a kanamycin resistance gene). Individual colonies were screened by colony PCR using OneTaq® DNA Polymerase (New England Biolabs), and positive clones were confirmed via Sanger sequencing. Plasmids were then extracted using Qiagen Plasmid Plus Mini, Midi, or Maxi kits (Qiagen, 12945), depending on yield requirements.

2.2.2. Plasmid Transfection

DNA Plasmid transfection was performed using Lipofectamine 2000 (Invitrogen, 11668500) following the manufacturer's protocol. Briefly, cells were seeded in a 96-well plate (Corning, 353075) at a density of 20,000 cells per well. A total of 16–24 h after seeding, for 96-well transfection, editor plasmids (250 ng), FP plasmids (100 ng) and guide RNA plasmids (100 ng epegRNA and 50 ng ngRNA) were mixed with 0.55 μ l of Lipofectamine 2000. The DNA–lipid complexes were brought to a final volume of 25 μ l using Opti-MEM reduced serum medium (Gibco, 31985070), full transfection schemes found in Supplementary information 2. At 72 h post-transfection, GFP and RFP fluorescence were measured by flow cytometry using a CytoFLEX S system (Beckman Coulter), with gating done according to (Schene et al., 2022).

2.2.3. Isolating and Genotyping Sorted Cells

Genomic DNA from sorted cells was extracted using the Quick-DNA Microprep Kit (Zymo Research) following the manufacturer's protocol. Target loci were amplified by PCR using Q5® High-Fidelity DNA Polymerase (New England Biolabs), and PCR products were purified using the QIAquick PCR Purification Kit (Qiagen), also according to the manufacturer's instructions. Purified amplicons were submitted to EZSeq (Macrogen Europe) for Sanger sequencing. All PCR and sequencing primers are listed in Supplementary information 1.

2.2.4. Next Generation Sequencing of DNA Samples

Target regions flanking the editing site were amplified in a two-step PCR protocol using Q5 High-Fidelity DNA Polymerase (NEB) following the manufacturer's protocol. In the first reaction (PCR1), primers unique to the mHADHA mutation with Illumina adapter overhangs (Supplementary information 1) were used to generate amplicons. The 25 μ L PCR mixture included 12.5 μ L NEBNext Ultra II Q5 Master Mix, 0.125 μ L of each 100 μ M primer, 1 μ L genomic DNA, and nuclease-free water. Following PCR1, products were cleaned using magnetic bead-based size selection with AMPure XP

beads (Beckman Coulter). Beads were added at a defined volumetric ratio, mixed thoroughly by pipetting, and incubated at room temperature to allow DNA binding. After magnetic separation, supernatants were removed, and beads were washed twice with freshly prepared 70% ethanol. DNA was eluted in nuclease-free water. Cleaned PCR1 products were used as input (1 μ L) for the indexing reaction (PCR2), which used appended unique Illumina TruSeq barcode combinations to each sample for multiplexed sequencing. PCR2 followed the same cycling parameters and was also followed by AMPure XP bead purification to remove excess primers and small fragments. DNA concentrations were quantified using a Qubit 4 fluorometer with the dsDNA HS Assay Kit (Thermo Fisher Scientific). Purified libraries were normalized, pooled equimolarly, and sequenced on an Illumina iSeq 100 instrument. FASTQ files (Supplementary Data 1) were analysed using the RGEN Prime Editing (PE) Analyzer pipeline. Reads were aligned against both the wild-type and edited reference sequences. Editing efficiency was calculated as the percentage of reads containing the exact intended edit, relative to total reads passing quality thresholds.

2.2.5. Cell Cultures Maintenance

HEK293T cells (ATCC, CRL-3216), Neuro-2a cells (ATCC, CCL-131) and Gesickle Producer 293T cells (Takara, 632617) were cultured in Dulbecco's modified Eagle medium (DMEM) plus GlutaMax (Life Technologies; 10569044) supplemented with 10% (v/v) fetal bovine serum (FBS). Cells were maintained at 37 °C with 5% CO₂. Cell lines were confirmed to be negative for mycoplasma during this thesis. Primary fibroblasts were isolated from the ear tissue of homozygous HADHA c.1528G>C knock-in mice. Cells were maintained in DMEM/F-12 (Thermo Fisher, Cat. No. 11320033) supplemented with 10% fetal bovine serum (FBS; Gibco), 1% non-essential amino acids (NEAA; Thermo Fisher), and 1% penicillin-streptomycin (Thermo Fisher). Cells were seeded in 24-well plates at densities of $2,5 \times 10^3$ and incubated at 37°C with 5% CO₂. Media was changed every 2–3 days. For passage, cells were washed with PBS and detached using 0,05% trypsin-EDTA (Thermo Fisher). Only early-passage fibroblasts (P3–P8) were used for transduction experiments.

2.2.6. PE-eVLP Production

Gesickle Producer 293T cells were plated at a density of $11,67 \times 10^6$ cells per flask in 20 ml of DMEM + 10% FBS media in T175 flask (Corning, 353136). A total of 18–24 h after seeding, a mixture of plasmids was transfected to producer cells with Lipofectamine 2000 (Invitrogen, 11668500). For production of v3b PE-eVLPs, plasmids expressing VSV-G (920 ng), wild-type MMLV Gag–Pol (6470,0 ng), Gag–COM–Pol (4600 ng), Gag–P3–Pol (970,6 ng), P4–PE and P4-PE6d (970,6 ng) and 10120,0 ng COM-pegRNAs were co-transfected to each T175 flask. A total of 40–48 h after transfection, supernatants were collected, centrifuged at 500g for 5 min, then the supernatant was filtered through 0.45- μ m polyvinylidene difluoride (PVDF) filter. For PE-eVLPs used with cultured cells, 5 \times PEG-it Virus Precipitation Solution (System Biosciences, LV825A-1) was subsequently added to the supernatant to precipitate eVLPs overnight at 4 °C. The next day, the eVLPs were pelleted by centrifugation at 1,500g for 30 min at 4 °C and were concentrated 100-fold by resuspending in 230 μ l of PBS, and aliquoted in minimum volume of PBS solution to maximize the dose of PE-eVLPs within the permitted volume of injection. All eVLPs tested for optimization experiments in cell culture were concentrated uniformly using the above-mentioned method to facilitate direct comparison of PE-eVLP potency at the same volume of eVLPs transduced. For short-term storage, eVLPs were stored at 4 °C for up to 1 week. For long-term storage, eVLPs were stored at –80 °C and thawed on ice immediately before use. Repeated freeze–thaw was avoided.

2.2.7. PE-eVLP Transduction in Cultured Cells and Genomic DNA Collection

Target cells were plated at a density of 60000 cells per well in 48-well plates (Corning, 354509), 118000 cells per well in 24-well plates. A total of 18–24 h after seeding, PE-eVLPs were added to the media of target cells. Unless otherwise noted, cellular genomic DNA was collected 72 h after transduction. Briefly, medium was removed from each well and cells were washed with 1× PBS. Then 130 µl of lysis buffer (10 mM Tris–HCl pH 8.0, 0,05% SDS and 25 µg ml⁻¹ proteinase K) was added to each well. Following incubation at 37 °C for 1 h, the lysate was heated to 80 °C for 30 min and was used directly as an input for downstream genomic sequencing.

2.2.8. PE-eVLP Protein Content Quantification by ELISA

PE content in PE-eVLPs was quantified using the FastScan Cas9 (*Streptococcus pyogenes*) ELISA kit (Cell Signaling Technology, 29666C) following the manufacturer's protocol. A standard curve was generated using recombinant Cas9 (*S. pyogenes*) nuclease protein (New England Biolabs, M0386). The number of eVLPs per volume was measured by quantifying MLV p30 content and calculated by assuming that 20% of the measured p30 in solution is associated with VLPs and that each VLP molecule contains 1,800 molecules of p30 (Renner et al., 2020).

2.2.9. In-Fusion Cloning of P4–PE6 Construct

The P4–PE6 construct were generated by directional cloning into the linearized P4–PE vector backbone (Addgene #211375) using the In-Fusion® HD Cloning Kit (Takara Bio, #638910), following the manufacturer's protocol. The P4–PE vector (was linearized by restriction digestion with SspI (NEB, R0569S) and XhoI (NEB, R0146S) in 10× rCutSmart™ Buffer (NEB, B6004S) and extracted and purified using the Qiagen Plasmid Plus Midi kits (Qiagen, 12945). Insert fragments were designed with appropriate homology arms and synthesized via PCR. The final assembly included four PCR fragments with the following input quantities: 30 ng of PCR1 (1,371 bp), 99 ng of PCR2 (4,463 bp), 17 ng of PCR3 (755 bp), and 9 ng of PCR4 (406 bp), together with 45 ng of linearized vector backbone. In-Fusion reactions were performed using the In-Fusion® HD Cloning Kit (Takara Bio, #638910) in a total volume of 20 µl, deviating from the manufacturer's standard protocol. Reactions included the DNA components described above, 4 µl In-Fusion HD Enzyme Premix, and were adjusted to final volume with nuclease-free water. Following assembly, products were transformed into Stellar™ competent *E. coli* (Takara Bio) and plated on selective LB agar plates. Clones were screened by colony PCR and verified by Sanger sequencing. Following assembly, 2 µl of each reaction was transformed into Stellar™ competent *E. coli* (Takara Bio) via heat shock at 42 °C for 45 seconds. Cells were recovered in SOC medium at 37 °C for 1 hour with shaking and plated on LB agar plates supplemented with ampicillin or kanamycin (Sigma-Aldrich), depending on plasmid resistance. Plates were incubated overnight at 37 °C. Colonies were screened by colony PCR, and positive clones were verified by Sanger sequencing using U6 promoter and insert-specific primers. Plasmid DNA was isolated using either the PureLink™ Quick Plasmid Miniprep Kit (Thermo Fisher Scientific) or NucleoBond Xtra Midi/Maxi Kit (Macherey-Nagel), and concentrations were quantified by NanoDrop spectrophotometry (Thermo Fisher Scientific).

3. Results

3.1. FluoPEER Screen of epegRNA and PE System

The FP screening was conducted using two primary designs of epegRNAs: one set designed to repair the HADHA c.1528G>C mutation, and another set designed to introduce this mutation. Complete epegRNA designs, including spacer, scaffold, and backbone sequences, are provided in Supplementary information 1. Details on transfection protocols are described in the Materials and Methods section. An overview of all FP screening conditions is presented in Table 1. Flow cytometry data were analyzed using the FloReada software package, with representative raw datasets and calculations included in Supplementary information 3.

3.1.1. Repair-epegRNA and PE Optimization Evaluation

To identify optimal epegRNA configurations for targeting the HADHA c.1528G>C mutation, a series of epegRNA designs was systematically screened using the FP dual-fluorescent reporter assay in HEK293T and N2a cells. Combinations of PBS and RTT lengths were first assessed (Figure 6a). In HEK293T cells, the P11R34 construct yielded the highest editing efficiency, as measured by both relative count (RFP⁺/GFP⁺) and mCherry/GFP fluorescence intensity. In contrast, overall editing rates in N2a cells were markedly low across all conditions. PE variants were compared (Figure 6b), with PE6d demonstrating improved activity over PEmax and other constructs in HEK293T cells, though gains in N2a cells were again more limited. Lastly, modifications to the epegRNA scaffold were evaluated (Figure 6c). EpegRNAs incorporating the COM scaffold extension showed a slight trend toward higher editing activity compared to both standard and MS2 scaffolds, particularly in HEK293T cells. This leaves the optimal epegRNA structure at an PBS length of 11, an RTT length of 34, incorporating a COM scaffold and utilizing PE6d.

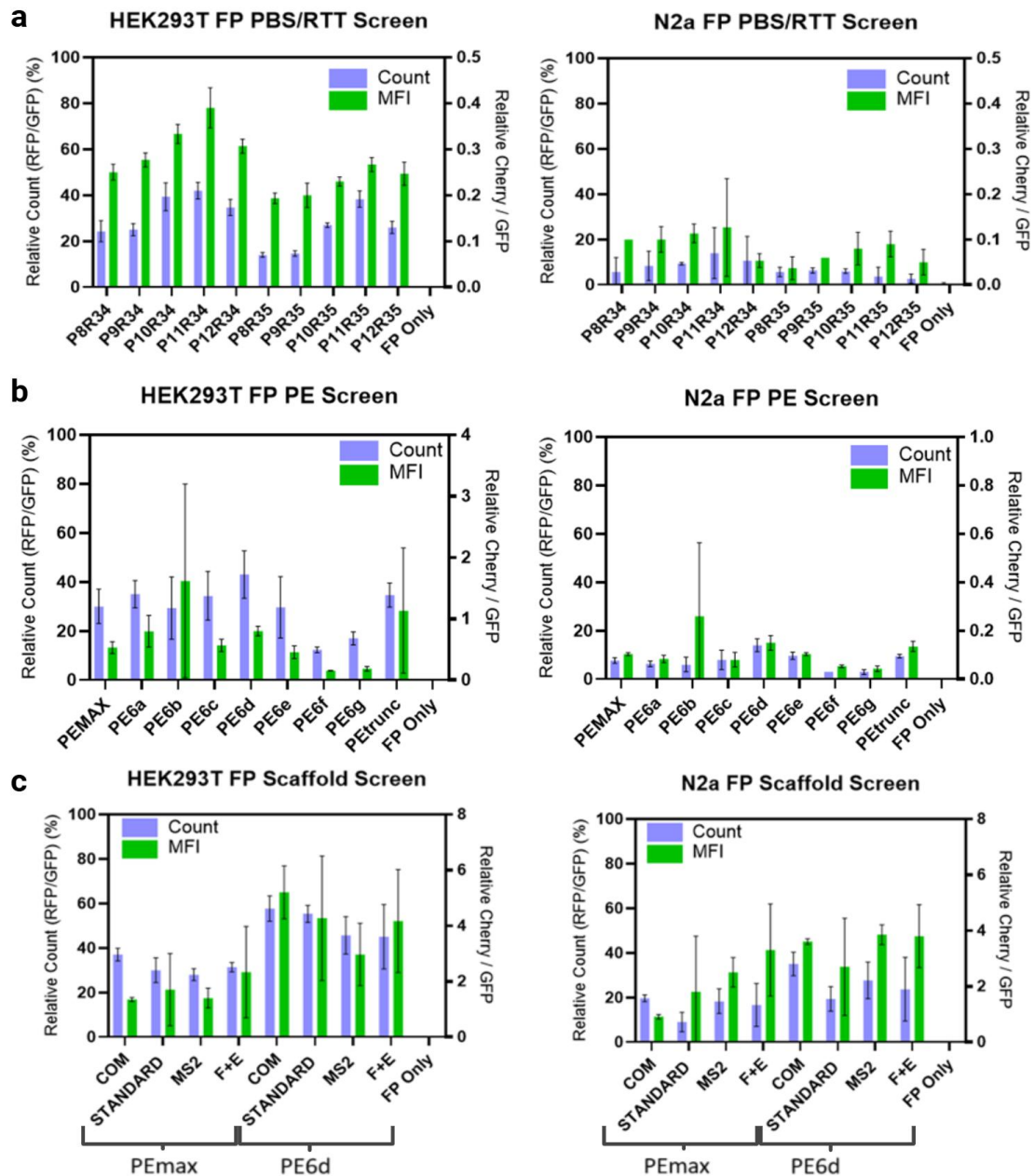


Figure 6. epegRNA Optimisation Screens for *mHADHA* c.1528 C>G using the FP Reporter Assay.
a PBS/RTT length screen. Bar plots show relative editing efficiency of epegRNAs with varying PBS and RTT lengths in HEK293T (left) and N2a (right) cells. Editing was quantified by two metrics: relative count (RFP⁺/GFP⁺ cells; blue) and relative mCherry/GFP fluorescence intensity (green). **b** PE variants screen. Editing performance of multiple PE variants (PEmax, PE6, PE6d, PE6g, PE6e, PE6f, PEtrunc) was evaluated in combination with a fixed epegRNA (P11R34, STANDARD scaffold) in HEK293T (left) and N2a (right) cells. **c** Scaffold screen. Relative editing efficiency of epegRNAs with different scaffold configurations (COM, MS2, F+E, STANDARD) was assessed using both PEmax and PE6d editor with again a fixed epegRNA (P11R34 - STANDARD scaffold) in HEK293T (left) and N2a (right) cells. In all panels, “FP only” refers to a transfection control lacking both epegRNA and PE. Error bars indicate standard deviation ($n = 3$ biological replicates). The exact sequences used in this study are provided in Supplementary information 1.

3.1.2. Create-epgRNA and PE Optimization Screen Evaluation

To validate the optimized epgRNA–PE combination in a genomic context, the mHADHA c.1528G>C mutation was introduced into healthy N2a cells using the fully optimized epgRNA design found until now (P11R34 / COM scaffold / PE6d), along with an RTT configured to install the mutation (create RTT). Further parameters named in Table 1 would thus include a fixed epgRNA (P11R34 / COM scaffold / PE6d / create RTT).

First, silent mutations were introduced to evade mismatch repair, aiming to improve retention of the intended edit. Among the variants tested, the CTA>CTG substitution showed the most promising results and was selected for further use in the optimal epgRNA design (Figure 7a). Next, another series of PEs were tested. These variants offered little gains compared to PE6d in both HEK293T and N2a cells (Figure 7b). To prevent re-cutting following successful editing, PAM-disrupting silent mutations (PAM-SM) were introduced. The TCG variant performed best across both cell lines, clearly enhancing editing efficiency compared to epgRNA without PAM-SM (Figure 7c). In parallel, a panel of nicking guide RNAs (ngRNAs) targeting the unedited strand was screened to bias the repair outcome toward the desired mutation. Among these, ngRNA5 yielded a great increase in editing on the FP plasmid compared to epgRNA without ngRNA (Figure 7d).

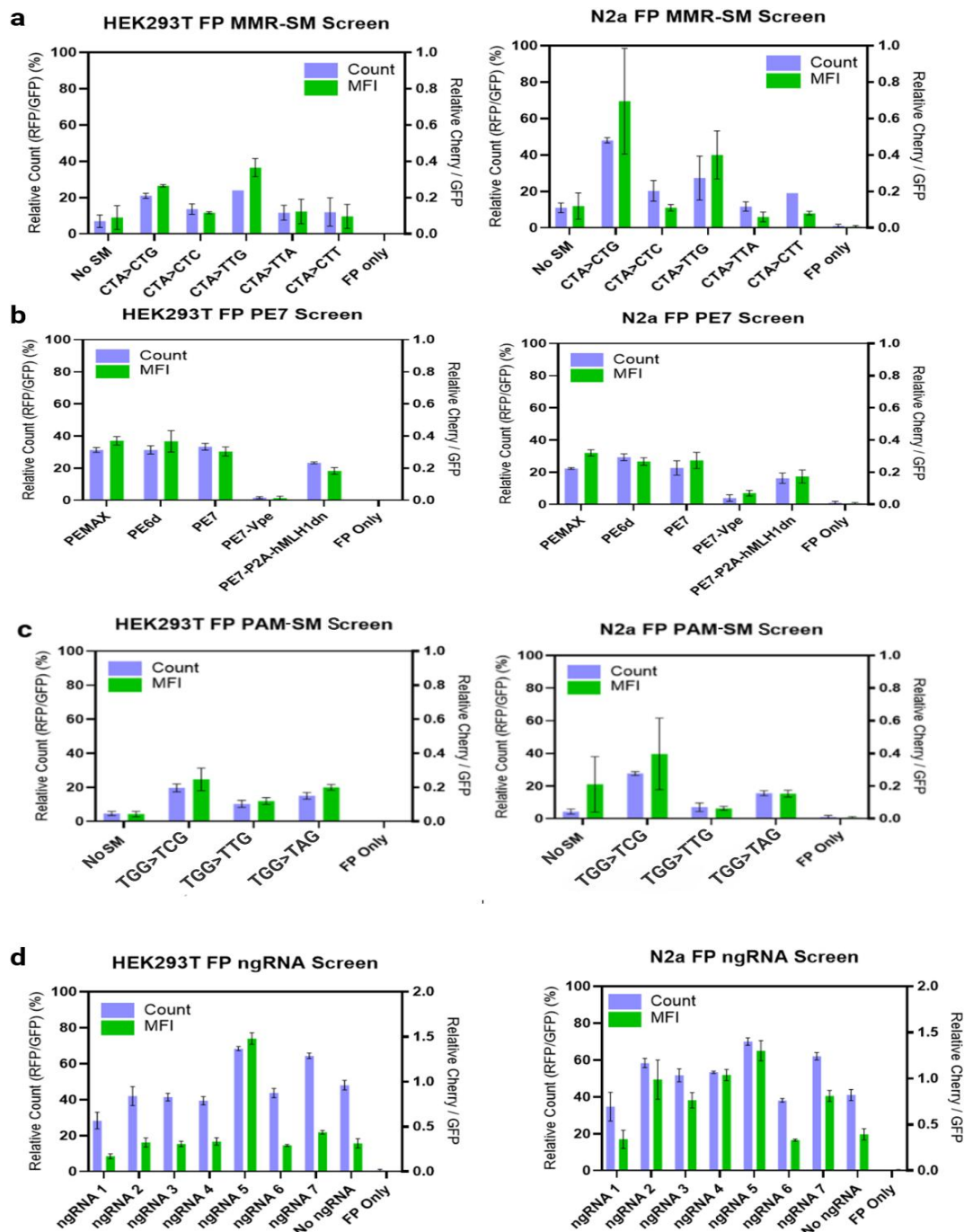


Figure 7. epegRNA Optimisation Screens for mHADHA c.1528 G>C using the FP Reporter Assay.

a MMR-SM screen. Variants of the fixed P11R34 / COM / PE6d epegRNA containing single codon substitutions (e.g., CTA>CTG, CTA>CTC) were evaluated for editing efficiency in HEK293T (left) and N2a (right) cells. **b** Second PE variants screen. Editing efficiency was compared between PE6d and PE7 constructs (PE7, PE7-Vpe, and PE7-P2A-MLH1dnH). **c** PAM silent mutation screen. PAM-disrupting variants (TCG, TTG, TAG) were tested to prevent post-edit re-cutting of the target sequence. **d** ngRNA screen. A panel of ngRNAs targeting the non-edited strand was assessed for their ability to enhance editing. ngRNA 5 refers to ngRNA 5 Old (Supplementary information 1). In all panels, editing efficiency was measured as relative count (RFP⁺/GFP⁺; blue) and relative mCherry/GFP fluorescence intensity (green). Error bars represent standard deviation (n = 3 biological replicates). "FP only" refers to FP plasmid-only control without editing components. The exact sequences used in this study are provided in Supplementary information 1.

However, it was later discovered that ngRNA 5 was designed to be complementary to the mHADHA c.1528 G>C genome, and not the FP plasmid. Since ngRNA 5 binds the wild-type DNA strand, and its binding site overlaps the intended edit, in this case the ngRNA would only bind to the FP plasmid after the edit had been inserted and the open reading frame restored. For this reason, the experiment was repeated, with the correct ngRNA 5 (ngRNA 5 New, Supplementary information 1) and with repair-epgRNA (Figure 8a). This setup allowed a valid comparison of ngRNA5's ability to enhance editing efficiency compared to the other ngRNAs. To assess the reliability of the initial findings (Figure 7d), as the result is quite unexpected and remarkable, the original ngRNA5 Old FP screen using create-epgRNA was repeated independently by a different researcher (Figure 8b). Additionally, a second independent experiment by the same researcher evaluated ngRNA5 New with the repair-epgRNA under multiple conditions (Figure 8c).

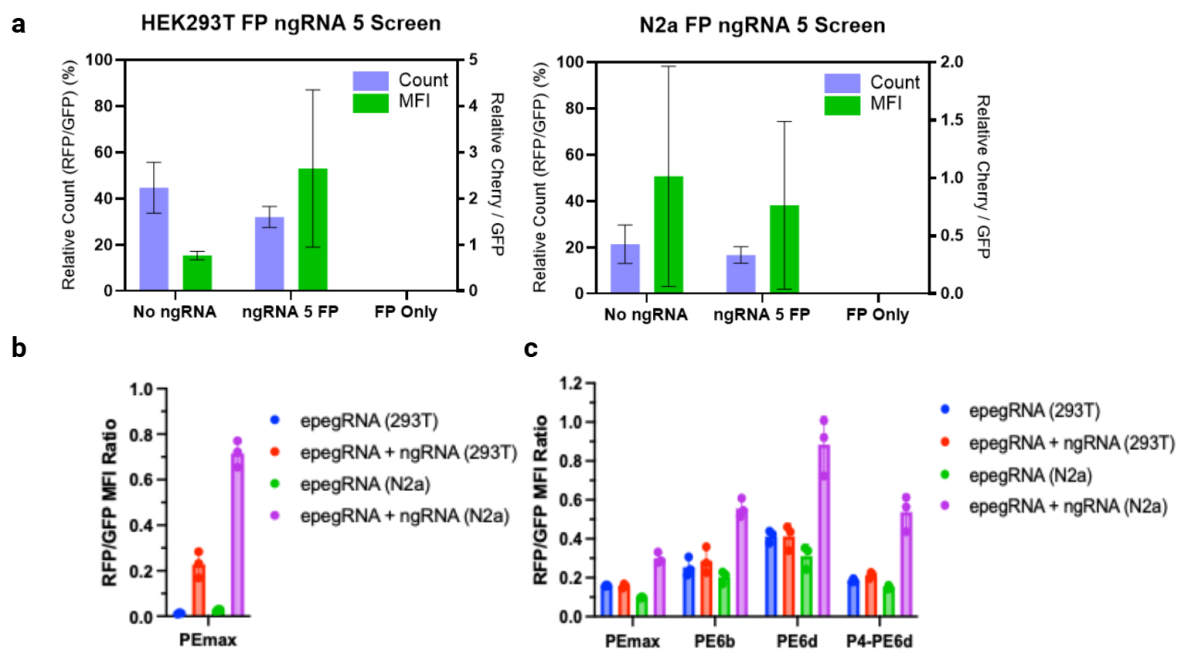


Figure 8. Second ngRNA 5 screen utilizing ngRNA 5 Old and ngRNA 5 New.

a FP screen testing ngRNA 5 New in combination with the repair-oriented epegRNA (P11R34-COM scaffold-PE6d-repair RTT) in HEK293T and N2a cells. **b** Independent experiment repeating the original setup, in which ngRNA 5 Old was tested with a create-oriented epegRNA. **c** Independent screen testing ngRNA 5 New with the repair-epgRNA (p11r34-COM-repair RTT) across multiple PE variants (PEmax, PE6b, PE6d, and P4-PE6d) in HEK293T and N2a cells.

3.1.3. Impact of Edit Directionality on Prime Editing Efficiency

To evaluate whether prime editing efficiency is influenced by the directionality of the intended edit, inducing (create) versus correcting (repair) the HADHA c.1528G>C mutation, a direct comparison was performed using matched epegRNA configurations in HEK293T and N2a cells. Two distinct epegRNAs were employed: one without an MMR-SM, and one incorporating a CTA>CTG substitution. While the latter was originally designed to enhance editing retention by evading MMR, in this context it served as an independent second epegRNA to confirm the outcome of the create–repair screen. In both HEK293T and N2a cells, the repair-epegRNA had higher Relative Count and Relative Cherry/GFP than create-oriented epegRNA when no MMR-SM was present (Figure 9). Upon incorporation of the CTA>CTG MMR-evading mutation, editing efficiency for the create configuration exceeded that of repair.

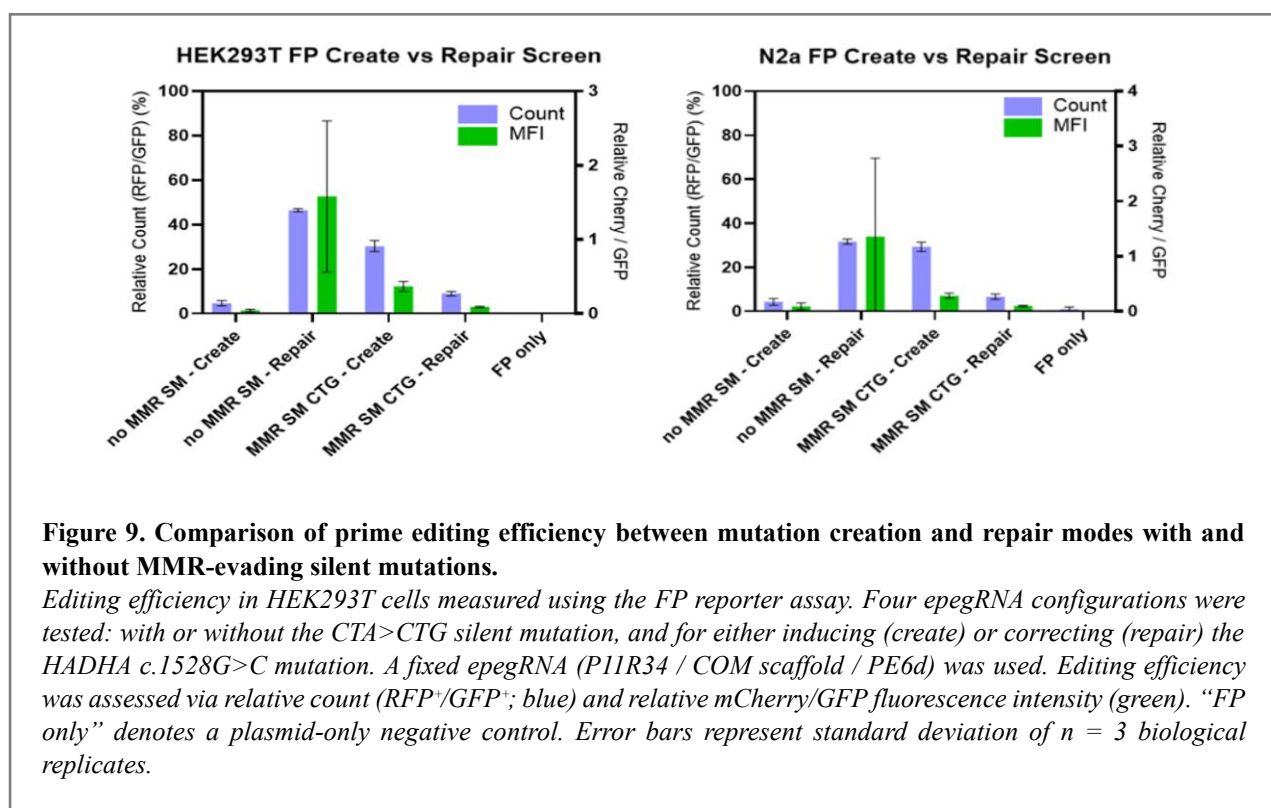


Figure 9. Comparison of prime editing efficiency between mutation creation and repair modes with and without MMR-evading silent mutations.

Editing efficiency in HEK293T cells measured using the FP reporter assay. Four epegRNA configurations were tested: with or without the CTA>CTG silent mutation, and for either inducing (create) or correcting (repair) the HADHA c.1528G>C mutation. A fixed epegRNA (P11R34 / COM scaffold / PE6d) was used. Editing efficiency was assessed via relative count (RFP⁺/GFP⁺; blue) and relative mCherry/GFP fluorescence intensity (green). “FP only” denotes a plasmid-only negative control. Error bars represent standard deviation of n = 3 biological replicates.

3.2. Genomic Analysis of epegRNA-PE System Functionality

3.2.1. Induction of mHADHA Mutation in N2a Using Create-epegRNA

Following the FP reporter assay screening data, the optimized epegRNA and PE combination was applied to introduce the mHADHA c.1528G>C mutation at the genomic level in N2a cells. The (P11R34 / COM scaffold / PE6d / CTA>CTG MMR-SM / ngRNA6 / create RTT) epegRNA PE combination was used to transfect N2a cells via lipofection (transfection scheme see Supplementary information 2). Using the FACS to isolate RFP⁺ cells, editing efficiency was assessed using both Sanger sequencing (Figure 10a) and next-generation sequencing (NGS) (Figure 10b). Sanger sequencing showed editing in the treated group, with frequency 16% for sample 1, and 0% for the two other samples. No editing was observed in the control condition, which consisted of untransfected N2a cells. NGS analysis of sample 1 however showed no editing.

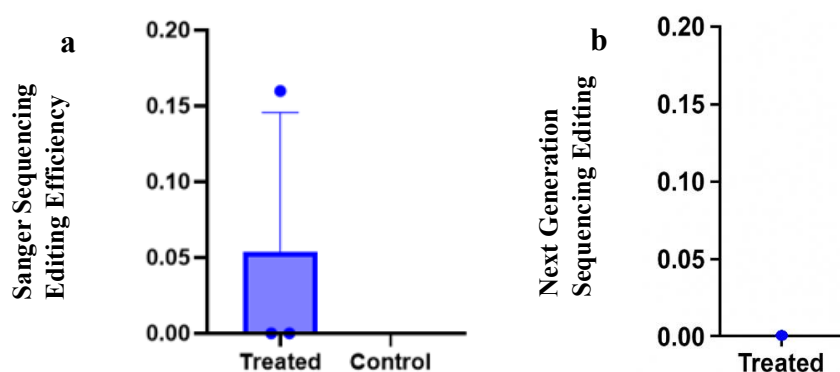


Figure 10. Sequencing Results of induction of mHADHA c.1528G>C mutation.

a Sanger Sequencing–based quantification of editing efficiency following induction of the HADHA c.1528G>C mutation in N2a cells. The bar plot shows editing efficiency in treated versus control conditions. Cells were transfected with the create-epegRNA-PE system (P11R34 / PE6d / COM / CTA>CTG / ngRNA6 / create RTT), followed by RFP⁺ cell sorting and genotyping. The Control condition consists of untransfected N2a cells. Individual biological replicates are shown as dots; error bars represent replicates ($n = 3$) **b** NGS sequencing result of sample 1.

3.2.2. V3b-VLP-Mediated Delivery of epegRNA into LCHADD Fibroblasts

To investigate the applicability of earlier made V3b-VLP-based prime editing for therapeutic correction of the c.1528G>C mutation in LCHADD, a transduction experiment using mouse-derived LCHADD fibroblasts was done. Using previously validated repair-epegRNA (P11R34 / COM / repair RTT) in combination with a new P4-PE6d PE construct. This editor plasmid was generated via In-Fusion cloning, using whole plasmid sequencing to confirm its integrity.

In addition to the primary test condition, V3b-VLPs loaded with the newly constructed P4-PE6d fusion protein and the validated mHADHA repair-epegRNA (P11R34 / COM / repair RTT), the experimental design incorporated several VLP-based control conditions:

A pegRNA control: P4-PEmax combined with mHADHA repair-epegRNA to test the epegRNA using a PE that is known to work.

A PE control: P4-PE6d combined with DNMT1-targeting epegRNA. This epegRNA has been optimized to target the DNMT1 gene and has been targeted in literature before (Anzalone et al., 2019). Lastly, an

eVLP Control: P4-PEmax combined with DNMT1-targeting epegRNA. This control is established to test whether the eVLP production was adequate. If no editing is observed in this control, either the VLP concentration was not high enough to induce an edit, or something went wrong with the production. Although plasmid assembly and initial packaging proceeded as expected, the experiment could not be completed due to a technical disruption during the transduction workflow. As a result, no genomic editing readouts were obtained, and the performance of repair-epegRNA in LCHADD fibroblasts could not be evaluated. To assess whether VLP production was sufficient prior to transduction, ELISA quantification was performed to assess the number of VLPs. Results indicated low capsid protein concentrations, suggesting suboptimal VLP yield (Supplementary data 3).

4. Discussion and Future Research Recommendations

4.1. Repair-epgRNA Parameters Impact in FP Screens

4.1.1. PBS/RTT Length Impact on Repair-epgRNA Performance

Among the repair-epgRNA parameters tested, the combination of an 11-nt PBS and a 34-nt RTT yielded the highest FP editing in both the HEK293T and N2a screen, which somewhat confirms the hypothesis made of longer PBS lengths outperforming shorter PBS lengths. One possible explanation for the increased performance of this combination is that the 11-nt PBS supported more effective annealing, with shorter PBS lengths not long enough to counter the long RTT. Additionally, the 34-nt RTT may have generated a more stable 3' flap than the 35-nt length, which could have improved flap retention and editing.

For further testing, PBS sequences shorter than 8-nt, will likely impair binding to the target strand due to the long RTT ‘‘hanging’’ onto it. Because of this rationale, and the lower editing efficiency observed with shorter PBS lengths, further experimentation in this range appears unnecessary. It would be interesting to the effect of PBS length >12, as is done in literature, however a drop-off in efficiency is already seen at a PBS length of 12-nt, both with RTTs of 34 and 35 nucleotides, making further testing of longer PBS lengths redundant. Similar to other epgRNA optimisations, the effects are all cell dependent and may vary between more cell types. The difference between epgRNA performance can already be seen in all screens between HEK293T and N2a cell types.

4.1.2. Scaffold Impact on Repair-epgRNA Performance

In HEK293T cells, the results show a clear pattern: editing efficiency goes up as the scaffold becomes more optimized, especially when using PE6d. This pattern is harder to spot in the N2a cells. One possible reason is that epgRNAs seem to work less efficiently in N2a overall, something that showed up in other parts of this project too. CytoFLEX data showed no real differences in cell count across the different scaffold, editor, or PBS/RTT screens, so cell loss probably isn't the cause here. Despite this, the COM epgRNA consistently outperformed other epgRNAs in HEK293T cells, making it the most promising candidate moving forward. The STANDARD scaffold, representing the minimal unmodified baseline, showed the weakest performance, likely due to reduced Cas9 affinity and vulnerability to Pol III termination or RNA degradation. The MS2 scaffold, while originally developed for VLP packaging via MS2–MCP interactions, offers little benefit in the plasmid context and may even hinder performance due to added structural bulk, which likely resulted in the lower FP editing efficiency. In contrast, the F+E scaffold should increase editing regarding its technical improvements. The result is however mixed, as the F+E scaffold epgRNA performed similarly to the STANDARD scaffold epgRNA in HEK293T but did improve on editing in N2a cells. Finally, the COM scaffold replaces the bulky MS2 aptamer with a compact COM aptamer while retaining the F+E backbone. This design should minimize steric hindrance, which may enhance epgRNA stability, explaining why COM performs on par with or better than F+E, especially in the PE6d condition. These findings are broadly consistent with the initial hypothesis, which predicted a stepwise improvement in editing efficiency

with each successive scaffold design. As expected, later-generation scaffolds, particularly COM, outperformed the STANDARD scaffold, though performance differences between intermediate designs were context-dependent.

4.1.3. PE variant Impact on Repair-epgRNA Performance

Compared to PEmax, the PE6 variants showed a clear divide in performance. PE6a through PE6d consistently achieved higher editing efficiency, while PE6e through PE6g did not. The improved results with PE6a and PE6b may be due to their more compact reverse transcriptase domains, which are likely to reduce steric hindrance and allow better access of the PE to the FP plasmid. Although earlier studies suggested and it was hypothesized that PE6c, combining the beneficial mutations of both PE6a and PE6b, should outperform them, this was not the case in this FP screen,. This again shows that editing efficiency depends heavily on the specific system and target. PE6d, designed to improve on PEmax, did as was hypothesized, with editing levels clearly higher in HEK293T and slightly better in N2a. On the other hand, PE6e to PE6g introduced further changes to the RT, but none of them improved editing, and in fact, performance was lower across both cell types. PEtrunc, engineered to have a shortened RT domain, outperformed PEmax, suggesting that the smaller compact RT is also effective in this FP plasmid screen.

4.1.4. Future Research Regarding Repair-epgRNA Findings

Although the early epgRNA design (P11R34) showed baseline activity, the optimized combination of P11R34 with the COM scaffold and PE6d (P11R34/COM/PE6d) resulted in significantly enhanced editing efficiency across both cell lines tested (Figure 6c). In HEK293T cells, this optimized configuration improved editing by 93% based on the RFP⁺/GFP⁺ cell count and by 204% based on RFP⁺/GFP⁺ mean fluorescence intensity (MFI), compared to the original epgRNA. In N2a cells, the same design led to a 289% increase in count and a 98% increase in MFI relative to the epgRNA using the STANDARD scaffold and PEmax. These findings highlight the critical impact of scaffold and PE variant selection on editing outcomes.

Future research could benefit from more and a broader combinatorial screening of epgRNA parameters. Rather than testing individual parameters in isolation, this would mean empirically evaluating all combinations of PBS/RTT lengths, scaffold types, and PE variants. In our case, we chose to move forward with what performed best in each category (P11R34 for PBS/RTT, the COM scaffold, and PE6d) assuming that combining the top performers would lead to the strongest editing outcome. But that assumption might not always hold. It's entirely possible that a different PBS/RTT configuration, one that didn't perform well with COM, might work much better when paired with a different scaffold, like F+E. In other words, the relationship between epgRNA components isn't necessarily additive. More experiments like shown in Figure 6c, where more parameters are tested in combination, must be performed. Additionally, large high-throughput screening approaches could help uncover these unexpected interactions beforehand (Kim et al., 2021). This would save a lot of time and resources and would allow future research to focus on only the most promising combinations for experimental validation. Based on our current data, a logical starting point would be to explore how PBS/RTT length interacts specifically with scaffold type, as we observed that longer RTTs such as RTT34–35 performed particularly well with the COM scaffold but not consistently with others. This suggests that certain RTT lengths may benefit from the structural stability of COM, while shorter or more unstable RTTs might

be better suited to F+E or MS2 scaffolds. Additionally, future combinations could be grouped based on predicted epegRNA folding energy or GC content, as these parameters likely modulate how well a given scaffold or RT variant can stabilize the complex and resolve the flap. In this way, we can reduce the screening space not randomly, but by organizing it according to mechanistic compatibility. Machine learning models trained on large-scale prime editing datasets, such as those described by (Yu, Kim, Park, Kim, et al., 2023), can further support this approach by predicting the efficiency of epegRNA designs across different editor variants and cell types, allowing for more targeted and efficient combinatorial optimization.

4.2. Create-epegRNA Parameters Impact on FP screens

Multiple parameters influenced create-epegRNA activity in the FP screenings. The screens discussed below used a fixed epegRNA (P11R34 / COM scaffold / PE6d / create RTT), variations in MMR-SM, PAM-SM, and ngRNA context.

4.2.1. MMR-SM Impact on Create-epegRNA Performance

In the MMR-SM screen, CTA>CTG yielded the highest editing signal in N2a cells, but also increased editing compared to no MMR SM in HEK293T. While this result is consistent with previous reports of MMR-silencing increasing editing efficiency, its impact in HEK293T was unexpected given HEK293T's reported MMR deficiency (Panigrahi et al., 2012). This might be the reason we see higher editing of more MMR silent mutations in N2a cells compared to HEK293T. A plausible explanation for some editing differences in HEK293T is that HEK293T could still retain partial or context-dependent MMR activity. Alternatively, the added MMR-SMs may impact the thermodynamic stability of the 3' flap or affect polymerase activity. However, the hypothesis does not hold in this screen, as more distant MMR-SMs like CTA>TTG performed better than closer ones such as CTA>CTT. While all MMR-SMs tested here were positioned near the edit, this result suggests that proximity is not the only factor influencing effectiveness.

4.2.2. PE7 Variants Impact on Create-epegRNA Performance

PE variant screening showed no relevant gains beyond PE6d, with PE7, PE7-Vpe, and PE7-P2A-MLH1dn failing to exceed the baseline established by PE6d in either cell line. This suggests that, at least for this target and setup, PE6d has already reached maximum editing. In HEK293T cells, which are known to have partial mismatch repair (MMR) deficiency PE7 and PE7-P2A-MLH1dn, performed comparably to or slightly below PE6d. The addition of the La RNA-binding domain in PE7 appears to offer limited benefit in this background, which goes against the earlier made hypothesis of later generations of PE outperforming earlier generations. The reason for the poor PE7-P2A-MLH1dn performance is likely due to the MMR deficiency of HEK293T cells. In contrast, in N2a cells, PE7-P2A-MLH1dn outperformed the other variants, showing increased editing frequency and RFP signal intensity. This suggests that the active MMR suppression (via MLH1dn) is most effective in MMR-proficient cells.

4.2.3. PAM-SM Impact on Create-epegRNA Performance

Silent mutations that disrupt the PAM clearly affected editing efficiency. The TCG variant (TGG→TCG) gave the highest editing, likely because it fully disrupted the PAM without causing issues in local DNA structure or codon usage. This likely prevented Cas9 from re-binding the site after editing,

which would reduce re-cutting and help retain the edit. The TAG variant also improved editing noticeably, possibly for similar reasons, even though it encodes a stop codon. In this setup, it didn't seem to interfere with the RFP signal. On the other hand, the TTG variant showed lower editing. A likely explanation is that Cas9 still recognizes it as a weak PAM, which could lead to re-cutting of the FP plasmid, disrupting the RFP reading frame and lowering the signal. It's worth noting that only a few PAM-SMs are possible in this system. As discussed in the introduction, the PAM overlaps two codons, only changing the middle base can leave the amino acids unchanged, mutating the first or third base would change the protein sequence, which we want to avoid.

4.2.4. ngRNA Impact on Create-epgRNA Performance

In the initial FP ngRNA screen, several nicking guides were tested alongside create-epgRNAs to assess their ability to enhance editing efficiency. Among these, ngRNA7 and ngRNA5 showed the strongest effect in HEK293T cells, increasing both the RFP⁺/GFP⁺ cell count and the mCherry/GFP intensity compared to other guides and the no-ngRNA control. In contrast, multiple ngRNAs performed well in N2a cells, likely reflecting cell-type-specific differences in repair pathways. The hypothesis that ngRNAs positioned closer to the edit site enhance editing efficiency does not entirely hold. ngRNA7 clearly outperformed both ngRNA6 and ngRNA1 in HEK293T and N2a cells and was outperformed only by ngRNA5 in HEK293T. In follow-up experiments using the corrected version of ngRNA5 (Fig. 7a and 7c), a similar enhancement in editing signal was observed, most notably in N2a cells. This further highlights the influence of cellular context on ngRNA performance. These results suggest that ngRNAs 2, 3, 4, 5, and 7 are promising candidates for future combinatorial screens, where repair-epgRNAs can be systematically tested in combination with these guides to build on the results already obtained from the create-epgRNA screens.

One unexpected result emerged from the initial create-epgRNA screen: ngRNA5 Old, which contained a design flaw and was only complementary to the edited DNA sequence, still led to a strong editing signal. This was surprising, as it should not have been able to bind or function effectively in unedited plasmids. To verify the finding, the same condition was repeated by an independent researcher using the original plasmids and transfection setup. The elevated RFP⁺/GFP⁺ signal was reproduced, confirming that the effect is genuine and not the result of experimental error. There are two possible explanations for this outcome.

The first is that ngRNA5 Old still binds the unedited DNA despite its single-nucleotide mismatch, perhaps due to some degree of mismatch tolerance in the guide–target interaction. If so, it would be unusually efficient despite the imperfect match, which stands in contrast to most findings in prime editing, where stronger guide–target binding typically correlates with better editing outcomes.

A more likely and interesting alternative is that ngRNA5 Old only binds after the intended edit is installed. In this scenario, the nick introduced by ngRNA5 could re-engage the cell's repair machinery, triggering a second round of repair that resolves residual imperfections such as flap structures, mismatches, or partially repaired intermediates. It is possible that the initial prime editing event restores the open reading frame just enough to allow weak or unstable expression of mCherry, but not at a level sufficient to cross the detection threshold in the FP reporter assay. Once the nick is introduced post-edit, the additional repair step may correct any lingering defects in the edited region, resulting in a cleaner, more stable construct. Single-strand breaks, such as those induced by ngRNAs, are known to engage high-fidelity repair pathways, which are likely triggered in this context as well. This could boost mCherry translation and enhance fluorescent signal intensity. In this way, ngRNA5 may amplify the functional readout of editing by improving the quality, not the quantity, of edited plasmids.

4.2.5. Future Research Regarding Create-epgRNA Optimisation

Aside from future research potential already discussed in section 4.1, MMR-SM findings in HEK293T warrant deeper investigation. Although HEK293T cells are known to be partially MMR-deficient, the MMR-silent mutation still led to a noticeable increase in editing efficiency, which raises questions about the underlying mechanism. To investigate this further, follow-up experiments could include comparing results in fully MMR-deficient versus MMR-proficient HEK293T cell lines. This would help determine whether the observed gains are truly linked to residual MMR activity, or whether other mechanisms, such as repair pathway bias or improved 3'-flap stability, are responsible. Other MMR-SMs are possible, as the RTT provides sufficient sequence space to introduce additional changes. However, literature suggests that MMR-SMs positioned closest to the edit site tend to yield the highest editing efficiency. In particular, the three nucleotides immediately downstream of the edit represent a promising region for further optimization. Since this study focused only on introducing MMR-SMs in the three nucleotides upstream of the edit, it remains an interesting future research question whether incorporating downstream mutations could enhance editing efficiency, and even more interesting if additional SMs, downstream or upstream could increase editing efficiency even more. Furthermore, this study showed that proximity to the edit might play a smaller role than hypothesised, it would be interesting for future studies to explore mutations placed further from the edit to see whether the original hypothesis could still apply over longer distances.

More research into PAM-SM will be limited, as changes to the first or third nucleotide of the PAM would induce undesirable amino acid change (Figure 5b).

To further investigate the strange outcome of the first ngRNA experiment, in context of ngRNA5, it would be interesting to test how many mismatches ngRNAs can tolerate. NgRNAs could possibly function even with a mismatch, which opens the option that perfect alignment may not always be necessary. In the context of this research however, ngRNA 5 must be tested on a genomic level, to see if these strange FP findings also translate into higher genome editing. Furthermore, the setup of ngRNA 5 is worth repeating in a slightly different form. Other ngRNAs could be designed to overlap the edit site and tested to see whether they also increase fluorescent signal when introduced after the edit is installed. If similar effects are observed, it would support the idea that post-edit nicking can trigger a useful second round of repair. To take it a step further, this approach could also be tested on a genomic target. That would help determine whether the effect is unique to the FP plasmid system or whether it can also improve editing outcomes at the genomic level.

4.3. epgRNA Directionality FluoPEER Screen

A clear directional bias in editing was observed when create- and repair-epgRNA were screened: epgRNAs designed to repair the HADHA c.1528G>C mutation (switching mutant C back to wild-type G) consistently outperformed those that created the mutation (G to C), and this held true in both HEK293T and N2a cells. When we added a mismatch repair-evading silent mutation (CTA→CTG) near the edit site, the asymmetry became even more obvious—it helped the create-epgRNA, which matched earlier MMR-SM FP results, but surprisingly, it made the repair-epgRNA perform much worse. What's striking is that these pegrRNAs differ by just one base, and they're at the exact same position in an otherwise identical RTT and PBS. It's also not just mismatch repair, as discussed earlier, HEK293T cells don't have a functioning MMR system, and yet a trend is observed of repair-epgRNA achieving higher editing on FP than create-epgRNA. That means the difference must come down to

something subtler: the identity of the base being written (C vs G). This one nucleotide difference was also observed earlier during the second PE screen (Figure 7b). PE6d and PEmax performed similarly here, which contradicts earlier observations of PE6d outperforming PEmax (Figure 6b). However, those initial comparisons were made using a repair-epegRNA, instead of create-epegRNA, again highlighting that directionality may influence the editing outcome.

The difference could make sense from a biochemical perspective. It's possible that the repair-epegRNA simply forms a cleaner, more stable 3' flap, while the create-epegRNA introduces a slight structural imbalance that disrupts resolution even though the guide sequence is nearly identical. Because even a single nucleotide can shift RNA folding or base-pairing dynamics, such a change might subtly affect how the epegRNA is presented to Cas9 or how the RTT is exposed during reverse transcription. Recent work has shown that seemingly minor alterations in the RTT, including silent changes, can have a surprisingly strong impact on editing outcomes by influencing both flap stability and how repair enzymes process the edited strand (Li et al., 2022).

4.3.1. Future Research Regarding Findings of epegRNA Directionality

For future research, this means that epegRNA optimization screens carried out using the create-configuration (MMR-SM, PAM-SM, ngRNA) be repeated with the corresponding repair-epegRNA. The FP screen on directionality shows that these optimizations do not translate directly across orientations, likely due the direction-specific effects. As a result, conclusions drawn from create-oriented screens may be biased and cannot reliably predict performance in repair-oriented screens.

4.4. Inflated MFI in Subset of FluoPEER Screenings

A recurring issue in the FP screening data is the unusually high MFI ratios observed in some screening samples, especially those with low cell counts. This effect is particularly noticeable in the PE screen (Figure 6b) and scaffold screen (Figure 6c), where certain samples show a disproportionately high mCherry/GFP⁺ ratio. Across multiple screens, the same pattern emerges. Low RFP⁺ cell counts often coincide with inflated FL1-A (RFP⁺) signal, which heavily distorts the overall trendline and weakens the statistical correlation. When comparing mCherry/GFP⁺ ratios to total RFP⁺ cells (Appendix 1), the relationship appears weak or inconsistent in multiple graphs. Repeating the experiment might seem justified, but this phenomenon is not an isolated event. Similar anomalies appear across other datasets as well (see Supplementary Information 3). These outliers seem to result either from abnormally low GFP signal or excessively high mCherry fluorescence, neither of which reliably reflects editing efficiency.

This distortion appears to stem from two phenomena. First, in samples with low overall cell counts, even minor measurement noise or gating inaccuracies can disproportionately affect MFI. A small number of highly fluorescent cells can dominate the mean value, skewing the ratio. Second, some samples with normal RFP⁺ cell counts still exhibit very high mCherry/GFP⁺ ratios often due to a greatly reduced GFP⁺ signal rather than inflated RFP. Possible explanations for these effects include stress-induced changes in membrane permeability, particularly in apoptotic or dying cells, which might enhance plasmid uptake and transiently boost fluorescence in a small subset. Alternatively, uneven plasmid uptake and distribution during transfection could lead to patchy overexpression, falsely raising the average MFI. As has already been done, filtering out implausibly high MFI values can mitigate

some effects, but must be done uniformly. While this strategy effectively removes the most extreme cases, it does not fully resolve the problem. Outliers that are not filtered during gating can still affect fluorescent ratios, especially when GFP signal is low, leading to misleading trends in the regression analysis. However, the FP plasmid system still showed clear and consistent trends across experiments, making it a useful tool for comparing different epegRNA and PE parameters, even with these limitations.

4.5. Mutation Induction in N2a using Create-epegRNA

The create epegRNA (P11R34 / COM / MMR SM CTA>CTG / ngRNA6) performed well in the FP screening but failed to induce detectable editing at the genomic HADHA locus in N2a cells. While one replicate initially showed ~16% editing based on Sanger sequencing (supplementary data 1, Figure 10a), this result was not replicated in NGS (supplementary data 2, Figure 10b), which revealed editing levels close to background. This discrepancy is normal between sanger sequencing and NGS, as sanger sequencing is known to be less accurate, and has a typical detection threshold around 15% variant allele frequency (VAF). Below this level, mixed chromatogram peaks become difficult to distinguish from background noise, often leading to either overestimation or complete failure to detect true edits (Rohlin et al., 2009). This contradicts the hypothesis that the editing capability of the optimized epegRNA–PE combination would also be detectable at the genomic level. One possible explanation for the prime editing failure could be the nature of the editing configuration itself. Although each component (COM scaffold, MMR-evading mutation, ngRNA, etc.), was independently optimized and shown to improve performance in screening, there's no guarantee they'll actually work better when combined. It's possible that the interplay between these features introduced unforeseen structural issues in the epegRNA or disrupted optimal timing between nicking and flap resolution. What works well in isolation does not always translate when multiple variables are stacked.

4.5.1. Future Research Regarding Induction of Mutation in N2a

For future research assessing epegRNA capability is far more useful to conduct in now available mHADHA fibroblasts, this approach leaves out directionality-related biases inherent to the “create” configuration discussed above and provides a more representative model for evaluating therapeutic editing outcomes.

4.6. Initial Attempts at VLP-Based Prime Editing Delivery

4.6.1. eVLP Usage Repair-epegRNA and PE Delivery into LCHADD Fibroblasts

In the mHADHA fibroblast model, the goal was to correct the c.1528G>C mutation using V3b VLPs carrying the repair-epegRNA and PE6d. However, this attempt also failed, as the fibroblasts died before successful transduction could occur. ELISA quantification confirmed that this VLP batch had a very

low particle count (Supplementary Data 3), as similar research used VLP concentration roughly 10x higher (An et al., 2024). A likely explanation for the low particle yield in both experiments is the VLP collection method. As precipitation rather than ultracentrifugation was used as a collection method, which may have reduced the final concentration or purity. To clarify whether this was the limiting factor, a direct comparison between precipitation and centrifugation-based VLP collection should be carried out in future experiments. This would help determine whether the low particle counts were caused by the collection method itself.

4.6.2. Future Research Regarding eVLP Usage for epegRNA and PE Delivery

Future experiments could include basic validation of VLP functionality prior to prime editing. For example, V3b VLPs carrying a GFP-encoding construct could be applied to fibroblasts to confirm that particles are successfully entering the cells and expressing their cargo. A dosing experiment with these GFP-VLPs on mHADHA fibroblasts would help determine the optimal particle input for efficient transduction. Once established, the V3b repair-epegRNA VLP delivery experiment can be repeated under these optimized conditions to assess genomic correction efficiency.

5. Acknowledgments

First of all, I am very grateful for my daily supervisor, Paul Schürmann, for guiding me through all the lab work over these past months., and for the continued advice on how to think and act like a good scientist. Also, my sincere gratitude to my study supervisor Bas Zwaan for continued mental and scientific support during our many online meetings. Finally, I like to thank everyone at the Fuchs lab from the RMCU for all their support and care.

I also acknowledge the use of OpenAI's ChatGPT (GPT-4) to support the editing and refinement of several thesis sections. Its assistance was limited to improving scientific writing clarity and phrasing, and did not replace or generate any original analysis, data, or conclusions. Further information is given in Appendix 2.

6. References

- An, M., Raguram, A., Du, S. W., Banskota, S., Davis, J. R., Newby, G. A., Chen, P. Z., Palczewski, K., & Liu, D. R. (2024). Engineered virus-like particles for transient delivery of prime editor ribonucleoprotein complexes in vivo. *Nature Biotechnology*, *42*(10), 1526–1537. <https://doi.org/10.1038/S41587-023-02078-Y>;SUBJMETA=1511,1647,2297,61,631;KWRD=GENETIC+ENGINEERING,PROTEIN+DELIVERY
- Anzalone, A. V., Randolph, P. B., Davis, J. R., Sousa, A. A., Koblan, L. W., Levy, J. M., Chen, P. J., Wilson, C., Newby, G. A., Raguram, A., & Liu, D. R. (2019). Search-and-replace genome editing without double-strand breaks or donor DNA. *Nature*, *576*(7785), 149–157. <https://doi.org/10.1038/S41586-019-1711-4>;TECHMETA=41,45;SUBJMETA=1511,1647,201,2110,61,631;KWRD=GENETIC+ENGINEERING,TARGETED+GENE+REPAIR
- Babcock, S. J., Curtis, A. G., Gaston, G., Elizondo, G., Gillingham, M. B., & Ryals, R. C. (2024). The LCHADD Mouse Model Recapitulates Early-Stage Chorioretinopathy in LCHADD Patients. *Investigative Ophthalmology & Visual Science*, *65*(6), 33–33. <https://doi.org/10.1167/IOVS.65.6.33>
- Banskota, S., Raguram, A., Suh, S., Du, S. W., Davis, J. R., Choi, E. H., Wang, X., Nielsen, S. C., Newby, G. A., Randolph, P. B., Osborn, M. J., Musunuru, K., Palczewski, K., & Liu, D. R. (2022). Engineered virus-like particles for efficient in vivo delivery of therapeutic proteins. *Cell*, *185*(2), 250–265.e16. <https://doi.org/10.1016/J.CELL.2021.12.021>
- Chai, D., Wang, J., Lim, J. M., Xie, X., Yu, X., Zhao, D., Maza, P. A. M., Wang, Y., Cyril-Remirez, D., Young, K. H., & Li, Y. (2025). Lipid nanoparticles deliver DNA-encoded biologics and induce potent protective immunity. *Molecular Cancer*, *24*(1), 12. <https://doi.org/10.1186/S12943-024-02211-8>/FIGURES/7
- Chatterjee, S., Kon, E., Sharma, P., & Peer, D. (2024). Endosomal escape: A bottleneck for LNP-mediated therapeutics. *Proceedings of the National Academy of Sciences of the United States of America*, *121*(11), e2307800120. <https://doi.org/10.1073/PNAS.2307800120/ASSET/753B2757-1D43-4A2A-AC8D-8BD68E7140F8/ASSETS/IMAGES/LARGE/PNAS.2307800120FIG03.JPG>
- Chauhan, V. P., Sharp, P. A., & Langer, R. (2024). Engineered prime editors with minimal genomic errors. *BioRxiv: The Preprint Server for Biology*. <https://doi.org/10.1101/2024.08.02.606370>
- Chen, P. J., & Liu, D. R. (2022). Prime editing for precise and highly versatile genome manipulation. *Nature Reviews Genetics* *2022* *24*:3, *24*(3), 161–177. <https://doi.org/10.1038/s41576-022-00541-1>
- Chew, W. L., Tabebordbar, M., Cheng, J. K. W., Mali, P., Wu, E. Y., Ng, A. H. M., Zhu, K., Wagers, A. J., & Church, G. M. (2016). A multifunctional AAV-CRISPR-Cas9 and its host response. *Nature Methods*, *13*(10), 868–874. <https://doi.org/10.1038/NMETH.3993>,
- Dean, D. A., Strong, D. D., & Zimmer, W. E. (2005). Nuclear entry of nonviral vectors. *Gene Therapy*, *12*(11), 881–890. <https://doi.org/10.1038/SJ.GT.3302534>,
- DeVine, T., Elizondo, G., Gaston, G., Babcock, S. J., Matern, D., Shchepinov, M. S., Pennesi, M. E., Harding, C. O., & Gillingham, M. B. (2024). iPSC-Derived LCHADD Retinal Pigment

- Epithelial Cells Are Susceptible to Lipid Peroxidation and Rescued by Transfection of a Wildtype AAV-HADHA Vector. *Investigative Ophthalmology & Visual Science*, 65(11), 22. <https://doi.org/10.1167/IOVS.65.11.22>
- Deyle, D. R., & Russell, D. W. (2009). Adeno-associated virus vector integration. *Current Opinion in Molecular Therapeutics*, 11(4), 442. <https://pmc.ncbi.nlm.nih.gov/articles/PMC2929125/>
- Doman, J. L., Pandey, S., Neugebauer, M. E., An, M., Davis, J. R., Randolph, P. B., McElroy, A., Gao, X. D., Raguram, A., Richter, M. F., Everette, K. A., Banskota, S., Tian, K., Tao, Y. A., Tolar, J., Osborn, M. J., & Liu, D. R. (2023). Phage-assisted evolution and protein engineering yield compact, efficient prime editors. *Cell*, 186(18), 3983. <https://doi.org/10.1016/J.CELL.2023.07.039>
- Doman, J. L., Sousa, A. A., Randolph, P. B., Chen, P. J., & Liu, D. R. (2022). Designing and executing prime editing experiments in mammalian cells. *Nature Protocols*, 17(11), 2431–2468. <https://doi.org/10.1038/S41596-022-00724-4>;SUBJMETA=1513,1647,1967,201,2110,3196,61,631;KWRD=CRISPR-CAS9+GENOME+EDITING,TARGETED+GENE+REPAIR
- Gao, Z., Ravendran, S., Mikkelsen, N. S., Haldrup, J., Cai, H., Ding, X., Paludan, S. R., Thomsen, M. K., Mikkelsen, J. G., & Bak, R. O. (2022). A truncated reverse transcriptase enhances prime editing by split AAV vectors. *Molecular Therapy*, 30(9), 2942–2951. <https://doi.org/10.1016/j.ymthe.2022.07.001>
- Gaston, G., Babcock, S., Ryals, R., Elizondo, G., DeVine, T., Wafai, D., Packwood, W., Holden, S., Raber, J., Lindner, J. R., Pennesi, M. E., Harding, C. O., & Gillingham, M. B. (2023). A G1528C Hadha knock-in mouse model recapitulates aspects of human clinical phenotypes for long-chain 3-hydroxyacyl-CoA dehydrogenase deficiency. *Communications Biology* 2023 6:1, 6(1), 1–12. <https://doi.org/10.1038/s42003-023-05268-1>
- Gillingham, M. B., Choi, D., Gregor, A., Wongchaisuwat, N., Black, D., Scanga, H. L., Nischal, K. K., Sahel, J. A., Arnold, G., Vockley, J., Harding, C. O., & Pennesi, M. E. (2024). Early diagnosis and treatment by newborn screening (NBS) or family history is associated with improved visual outcomes for long-chain 3-hydroxyacylCoA dehydrogenase deficiency (LCHADD) chorioretinopathy. *Journal of Inherited Metabolic Disease*, 47(4), 746–756. <https://doi.org/10.1002/JIMD.12738>
- Haapaniemi, E., Botla, S., Persson, J., Schmierer, B., & Taipale, J. (2018). CRISPR-Cas9 genome editing induces a p53-mediated DNA damage response. *Nature Medicine*, 24(7), 927–930. <https://doi.org/10.1038/S41591-018-0049-Z>;SUBJMETA=1427,1511,1513,1647,1967,337,631;KWRD=DNA+DAMAGE+AND+REPAIR,GENE+TARGETING,GENETIC+ENGINEERING
- Jang, H., Jo, D. H., Cho, C. S., Shin, J. H., Seo, J. H., Yu, G., Gopalappa, R., Kim, D., Cho, S. R., Kim, J. H., & Kim, H. H. (2021). Application of prime editing to the correction of mutations and phenotypes in adult mice with liver and eye diseases. *Nature Biomedical Engineering* 2021 6:2, 6(2), 181–194. <https://doi.org/10.1038/s41551-021-00788-9>
- Kahraman, A. B., Yildiz, Y., Gokmen-Ozel, H., Kadayifcilar, S., & Sivri, S. (2023). Successful management of rhabdomyolysis with triheptanoin in a child with severe long-chain 3-hydroxyacyl-coenzyme A dehydrogenase (LCHAD) deficiency. *Neuromuscular Disorders*, 33(4), 315–318. <https://doi.org/10.1016/j.nmd.2023.02.008>
- Kim, H. K., Yu, G., Park, J., Min, S., Lee, S., Yoon, S., & Kim, H. H. (2021). Predicting the efficiency of prime editing guide RNAs in human cells. *Nature Biotechnology*, 39(2), 198–206.

[https://doi.org/10.1038/S41587-020-0677-](https://doi.org/10.1038/S41587-020-0677-Y)
Y;SUBJMETA=1511,1513,1647,1967,3196,631;KWRD=CRISPR-
CAS9+GENOME+EDITING,GENETIC+ENGINEERING

- Li, X., Zhou, L., Gao, B. Q., Li, G., Wang, X., Wang, Y., Wei, J., Han, W., Wang, Z., Li, J., Gao, R., Zhu, J., Xu, W., Wu, J., Yang, B., Sun, X., Yang, L., & Chen, J. (2022). Highly efficient prime editing by introducing same-sense mutations in pegRNA or stabilizing its structure. *Nature Communications* 2022 13:1, 13(1), 1–9. <https://doi.org/10.1038/s41467-022-29339-9>
- Lu, R. M., Hsu, H. E., Perez, S. J. L. P., Kumari, M., Chen, G. H., Hong, M. H., Lin, Y. S., Liu, C. H., Ko, S. H., Concio, C. A. P., Su, Y. J., Chang, Y. H., Li, W. S., & Wu, H. C. (2024). Current landscape of mRNA technologies and delivery systems for new modality therapeutics. *Journal of Biomedical Science* 2024 31:1, 31(1), 1–36. <https://doi.org/10.1186/S12929-024-01080-Z>
- Maines, E., Gugelmo, G., Vitturi, N., Dianin, A., Rubert, L., Piccoli, G., Soffiati, M., Cauvin, V., & Franceschi, R. (2025). A Focus on the Role of Dietary Treatment in the Prevention of Retinal Dysfunction in Patients with Long-Chain 3-Hydroxyacyl-CoA Dehydrogenase Deficiency: A Systematic Review. *Children*, 12(3), 374. <https://doi.org/10.3390/CHILDREN12030374>
- Mohsen, M. O., & Bachmann, M. F. (2022). Virus-like particle vaccinology, from bench to bedside. *Cellular & Molecular Immunology* 2022 19:9, 19(9), 993–1011. <https://doi.org/10.1038/s41423-022-00897-8>
- Nelson, J. W., Randolph, P. B., Shen, S. P., Everette, K. A., Chen, P. J., Anzalone, A. V., An, M., Newby, G. A., Chen, J. C., Hsu, A., & Liu, D. R. (2022). Engineered pegRNAs improve prime editing efficiency. *Nature Biotechnology*, 40(3), 402–410. <https://doi.org/10.1038/S41587-021-01039-7>;SUBJMETA=1511,1647,201,2110,61,631;KWRD=GENETIC+ENGINEERING,TARGETED+GENE+REPAIR
- Neto, E. V., Wang, M., Szuminsky, A. J., Ferraro, L., Koppes, E., Wang, Y., Land, C. V. t., Mohsen, A. W., Zanatta, G., El-Gharbawy, A. H., Anthonyuthu, T. S., Tyurina, Y. Y., Tyurin, V. A., Kagan, V., Bayır, H., & Vockley, J. (2024). Mitochondrial bioenergetics and cardiolipin remodeling abnormalities in mitochondrial trifunctional protein deficiency. *JCI Insight*, 9(17). <https://doi.org/10.1172/JCI.INSIGHT.176887>
- Panigrahi, G. B., Slean, M. M., Simard, J. P., & Pearson, C. E. (2012). Human Mismatch Repair Protein hMutLa Is Required to Repair Short Slipped-DNAs of Trinucleotide Repeats. *The Journal of Biological Chemistry*, 287(50), 41844. <https://doi.org/10.1074/JBC.M112.420398>
- Patel, S., Ryals, R. C., Weller, K. K., Pennesi, M. E., & Sahay, G. (2019). Lipid nanoparticles for delivery of messenger RNA to the back of the eye. *Journal of Controlled Release : Official Journal of the Controlled Release Society*, 303, 91. <https://doi.org/10.1016/J.JCONREL.2019.04.015>
- Prasun, P., LoPiccolo, M. K., & Ginevic, I. (2022). *Long-Chain Hydroxyacyl-CoA Dehydrogenase Deficiency / Trifunctional Protein Deficiency*. <https://www.ncbi.nlm.nih.gov/books/NBK583531/>
- Renner, T. M., Tang, V. A., Burger, D., & Langlois, M.-A. (2020). Intact Viral Particle Counts Measured by Flow Virometry Provide Insight into the Infectivity and Genome Packaging Efficiency of Moloney Murine Leukemia Virus. *Journal of Virology*, 94(2). <https://doi.org/10.1128/JVI.01600-19/ASSET/0EACA056-0CA7-431F-8A8F-BE59E550F8A0/ASSETS/GRAPHIC/JVI.01600-19-F0007.JPEG>

- Rohlin, A., Wernersson, J., Engwall, Y., Wiklund, L., Björk, J., & Nordling, M. (2009). Parallel sequencing used in detection of mosaic mutations: Comparison with four diagnostic DNA screening techniques. *Human Mutation*, *30*(6), 1012–1020. <https://doi.org/10.1002/HUMU.20980>,
- Rücklová, K., Hrubá, E., Pavlíková, M., Hanák, P., Farolfi, M., Chrastina, P., Vlášková, H., Kousal, B., Smolka, V., Folténová, H., Adam, T., Friedecký, D., Ješina, P., Zeman, J., Kožich, V., & Honzík, T. (2021). Impact of newborn screening and early dietary management on clinical outcome of patients with long chain 3-hydroxyacyl-coa dehydrogenase deficiency and medium chain acyl-coa dehydrogenase deficiency—a retrospective nationwide study. *Nutrients*, *13*(9), 2925. <https://doi.org/10.3390/NU13092925/S1>
- Schene, I. F., Joore, I. P., Bajjens, J. H. L., Stevelink, R., Kok, G., Shehata, S., Ilcken, E. F., Nieuwenhuis, E. C. M., Bolhuis, D. P., van Rees, R. C. M., Spelier, S. A., van der Doef, H. P. J., Beekman, J. M., Houwen, R. H. J., Nieuwenhuis, E. E. S., & Fuchs, S. A. (2022). Mutation-specific reporter for optimization and enrichment of prime editing. *Nature Communications* *2022 13:1*, *13*(1), 1–10. <https://doi.org/10.1038/s41467-022-28656-3>
- Scholefield, J., & Harrison, P. T. (2021). Prime editing – an update on the field. *Gene Therapy*, *28*(7–8), 396–401. <https://doi.org/10.1038/S41434-021-00263-9>;TECHMETA=13,41,42;SUBJMETA=1511,1647,201,2110,61,631;KWRD=GENETIC+ENGINEERING,TARGETED+GENE+REPAIR
- Sharma, J., & Paschalis, E. I. (2022). The future of non-viral gene delivery for the treatment of inherited retinal diseases. *Molecular Therapy Nucleic Acids*, *30*, 354. <https://doi.org/10.1016/j.omtn.2022.10.011>
- Shirley, J. L., de Jong, Y. P., Terhorst, C., & Herzog, R. W. (2020). Immune Responses to Viral Gene Therapy Vectors. *Molecular Therapy*, *28*(3), 709–722. <https://doi.org/10.1016/j.ymthe.2020.01.001>
- Spiekerkoetter, U., Lindner, M., Santer, R., Grotzke, M., Baumgartner, M. R., Boehles, H., Das, A., Haase, C., Hennermann, J. B., Karall, D., de Klerk, H., Knerr, I., Koch, H. G., Plecko, B., Röschinger, W., Schwab, K. O., Scheible, D., Wijburg, F. A., Zschocke, J., ... Wendel, U. (2009). Management and outcome in 75 individuals with long-chain fatty acid oxidation defects: Results from a workshop. *Journal of Inherited Metabolic Disease*, *32*(4), 488–497. <https://doi.org/10.1007/S10545-009-1125-9>,
- Vockley, J., Burton, B. K., Berry, G., Longo, N., Phillips, J., Sanchez-Valle, A., Chapman, K. A., Tanpaiboon, P., Grunewald, S., Murphy, E., Lu, X., Rahman, S., Ray, K., Reineking, B., Pisani, L., & Ramirez, A. N. (2023). Triheptanoin for the treatment of long-chain fatty acid oxidation disorders: Final results of an open-label, long-term extension study. *Journal of Inherited Metabolic Disease*, *46*(5), 943–955. <https://doi.org/10.1002/JIMD.12640>,
- Yan, J., Oyler-Castrillo, P., Ravisankar, P., Ward, C. C., Levesque, S., Jing, Y., Simpson, D., Zhao, A., Li, H., Yan, W., Goudy, L., Schmidt, R., Solley, S. C., Gilbert, L. A., Chan, M. M., Bauer, D. E., Marson, A., Parsons, L. R., & Adamson, B. (2024). Improving prime editing with an endogenous small RNA-binding protein. *Nature*, *628*(8008), 639. <https://doi.org/10.1038/S41586-024-07259-6>
- Yu, G., Kim, H. K., Park, J., Kim, J., Kim, J., Kim, H. H., Kwak, H., Cheong, Y., & Kim, D. (2023). *Prediction of efficiencies for diverse prime editing systems in multiple cell types In brief An approach to identify the best guide RNAs for prime editing that couples insights from high-*

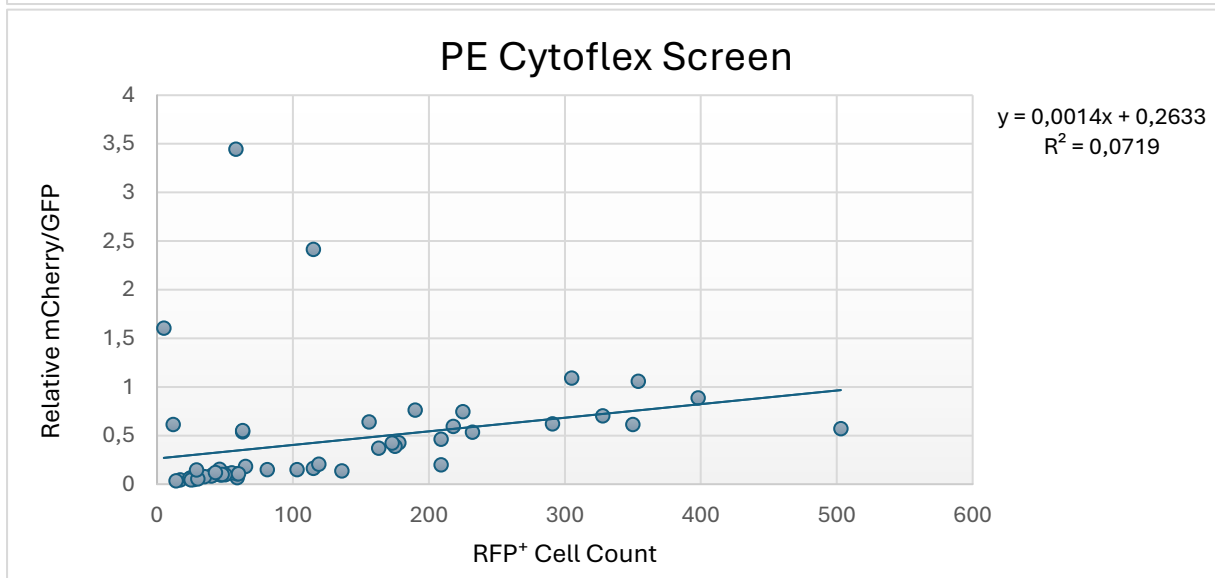
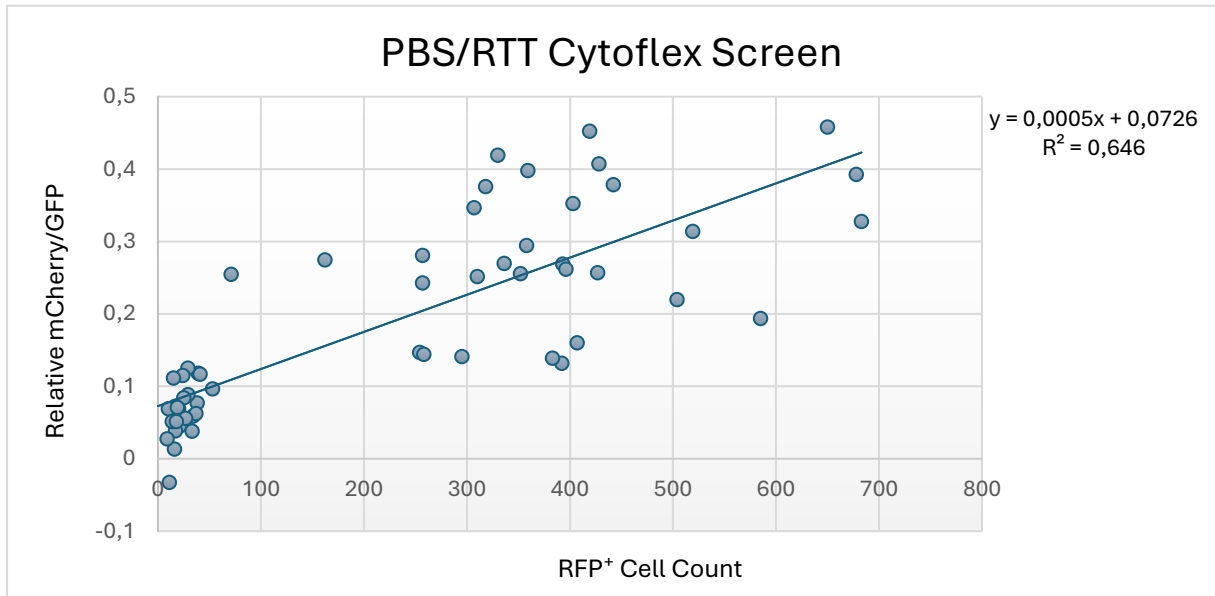
throughput analysis of >300,000 guide RNAs with deep learning. II Prediction of efficiencies for diverse prime editing systems in multiple cell types. <https://doi.org/10.1016/j.cell.2023.03.034>

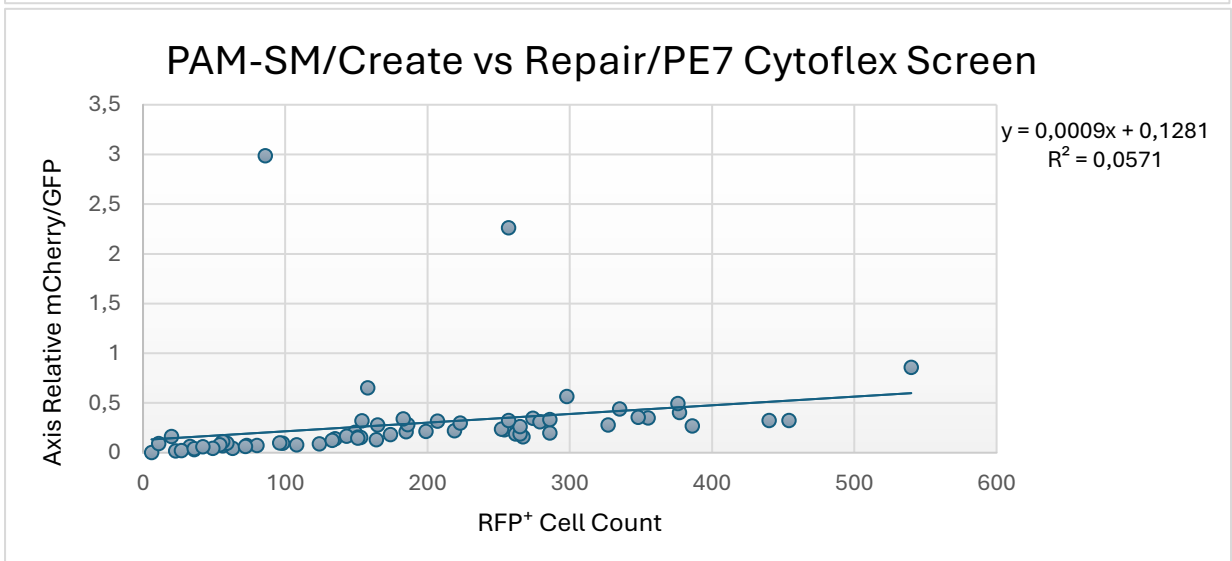
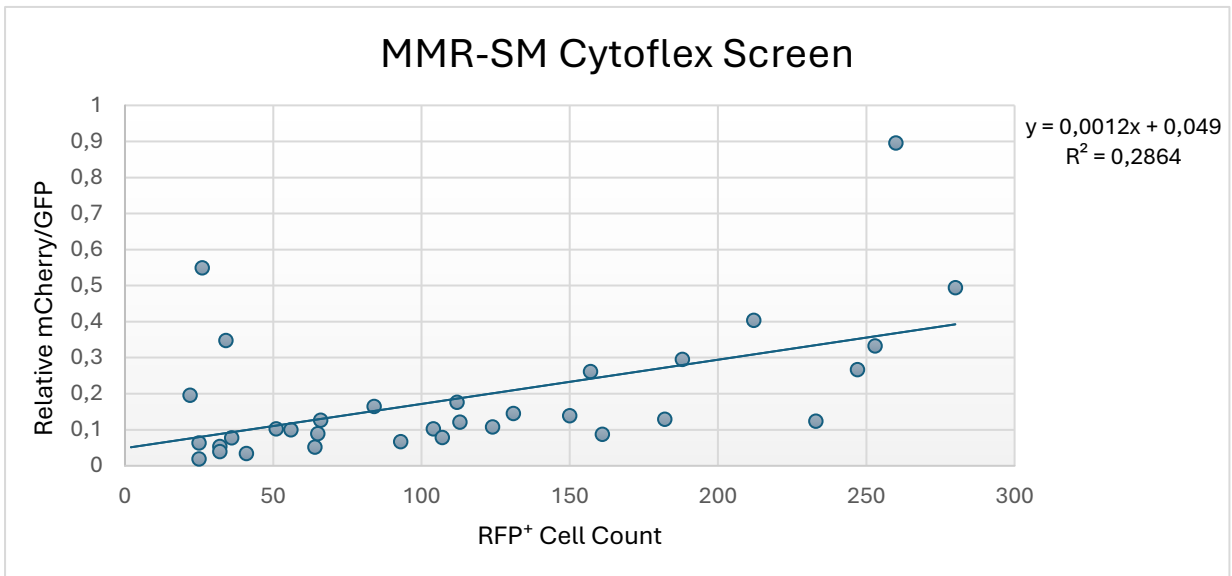
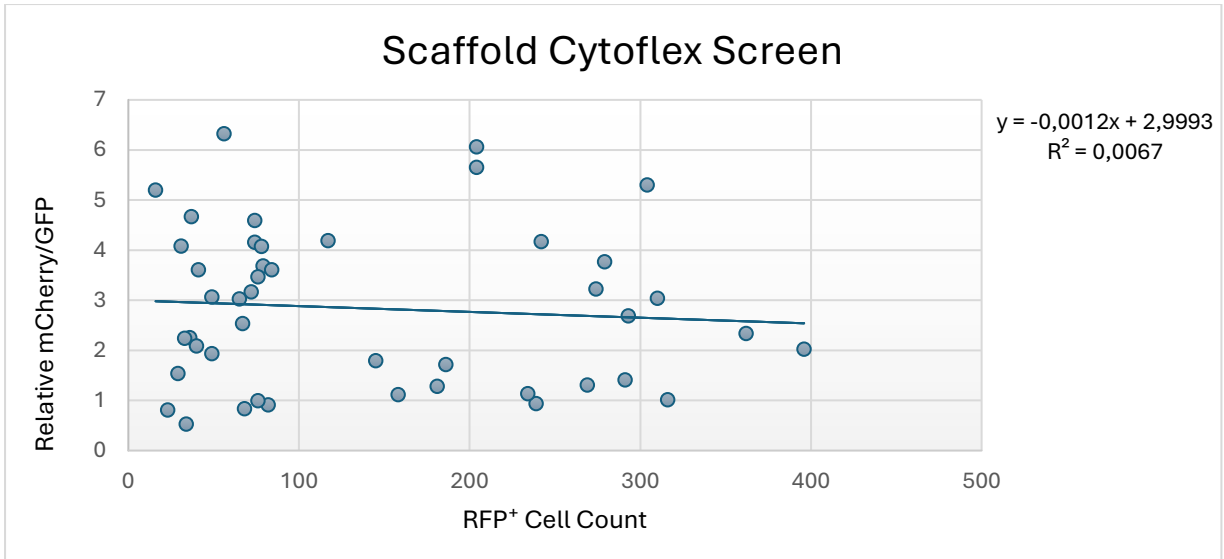
Yu, G., Kim, H. K., Park, J., Kwak, H., Cheong, Y., Kim, D., Kim, J., Kim, J., & Kim, H. H. (2023). Prediction of efficiencies for diverse prime editing systems in multiple cell types. *Cell*, 186(10), 2256-2272.e23. <https://doi.org/10.1016/J.CELL.2023.03.034>

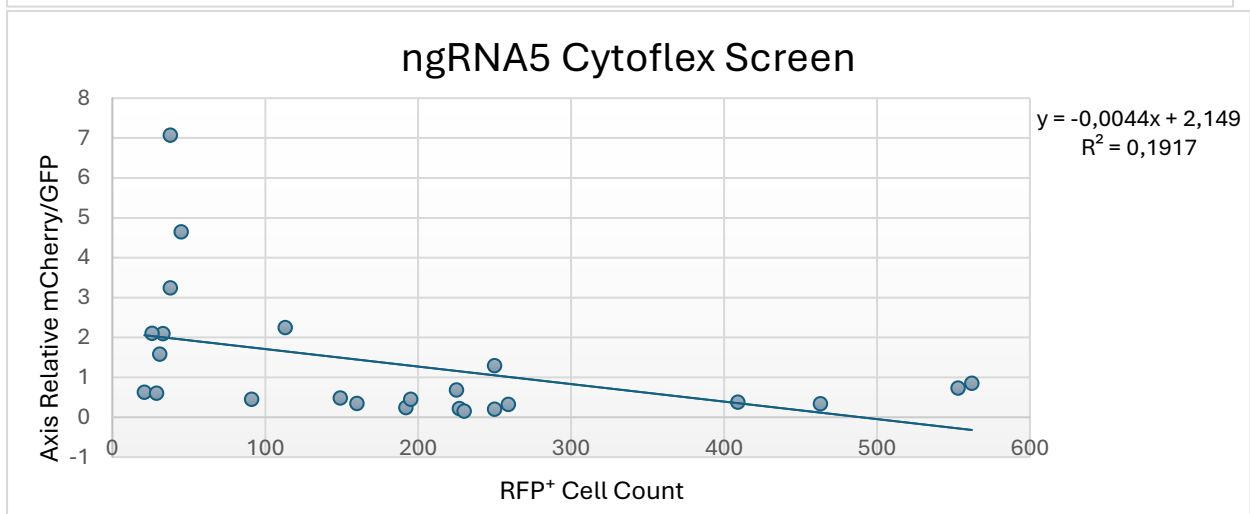
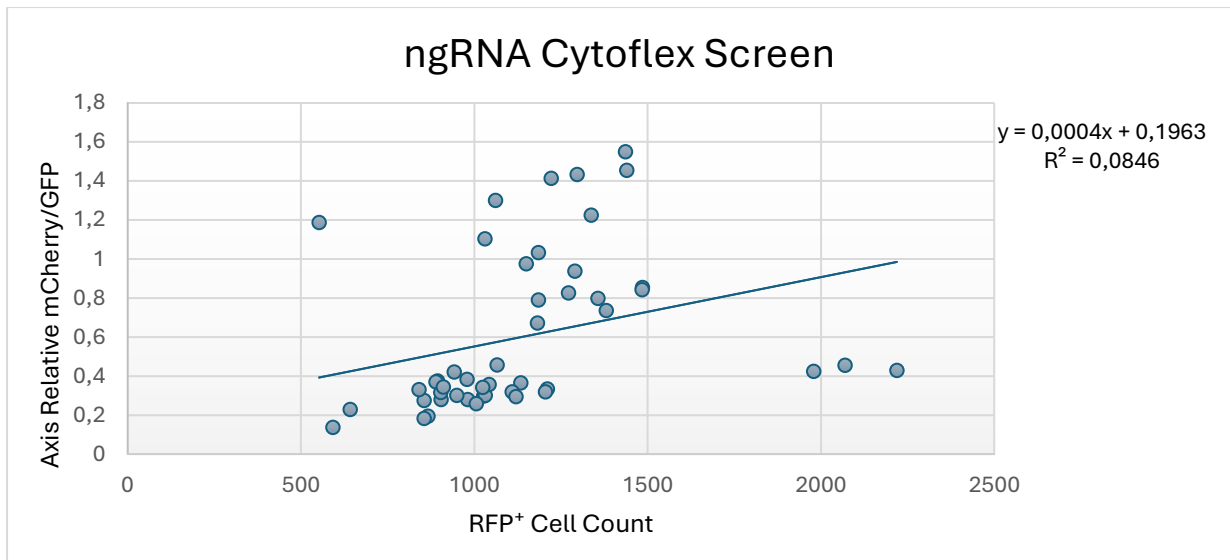
7. Appendix

Appendix 1

FP screening graphs plotting relative mCherry/GFP against RFP⁺ cells count. The graphs showcase the supposed linear relationship with increased RFP⁺ count and expected increased Relative mCherry/GFP.







Appendix 2

During the writing of this thesis, I used OpenAI's ChatGPT (GPT-4) to support several aspects of the writing and editing process. The tool was used to:

- Clarify complex molecular biology concepts, particularly related to prime editing, virus-like particles (VLPs), and lipid nanoparticle (LNP) delivery.
- Suggest phrasing improvements for increased scientific clarity and grammatical correctness.
- Rephrase or restructure technical paragraphs to meet academic tone.
- Assist in identifying appropriate primary sources and literature citations (all final sources were verified manually).

AI output was not used to generate raw experimental results, data interpretation, or novel scientific claims. All scientific conclusions and writing decisions were made by me, the author, and reflect my own understanding and intent. ChatGPT served as a language and structure refinement tool and was used with my own inputs and edits guiding each response. A detailed prompt log was retained privately and is available upon request for transparency. Due to system limitations, the original ChatGPT conversation cannot be linked directly.